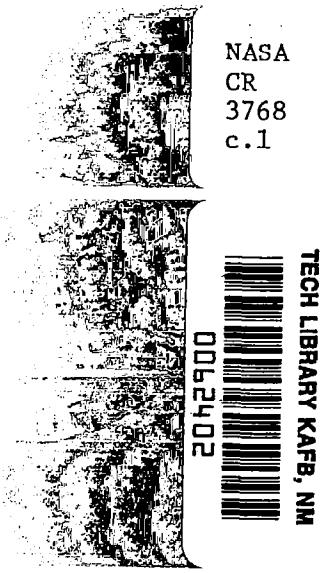

NASA Contractor Report 3768

Heat Generation in Aircraft Tires Under Braked Rolling Conditions

Samuel K. Clark and Richard N. Dodge

GRANT NSG-1607
JANUARY 1984

NASA

NASA Contractor Report 3768

Heat Generation in Aircraft Tires Under Braked Rolling Conditions

Samuel K. Clark and Richard N. Dodge
University of Michigan
Ann Arbor, Michigan

Prepared for
Langley Research Center
under Grant NSG-1607

NASA
National Aeronautics
and Space Administration

Scientific and Technical
Information Office

1984

SYMBOLS

English Letters

a	radius of tire cross-section
b	width of tire contact patch
c	tire circumference
$C_1 \ldots C_8$	constants
D	tire diameter
e	load offset dimension
$\bar{e}$	cord end count
F	force on axle
G	shear modulus of tire carcass
h	axle height
K_s	fore-aft spring rate of tire
l	contact path length
n	number of plies in tire
N	membrane forces in the carcass
p_o	inflation pressure
P	power
$\dot{Q}$	rate of heat release
$\dot{q}$	rate of heat release per unit volume
r	tire radius
s	tire slip
$\bar{s}$	cord spacing
t	carcass thickness
T	cord tension
T_o	torque on wheel
V	velocity of wheel axle
w	tread width
W	work done

Greek Letters

ε	strain
ϕ	angle
δ	deflection
γ	shear strain
τ	shear stress
α	cord angle

Subscripts

o	unbraked
b	braked
s	slip
x,θ	circumferential direction
z	vertical
ϕ	meridianal

INTRODUCTION

An analytical theory allowing the calculation of internal temperatures in free rolling aircraft tires has been described previously in ref. [1]. That theory was based on estimating the stress changes in various portions of a tire as each portion rolled through the contact patch, and then using those stress changes to estimate the corresponding rate of heat release from the known loss properties of the materials used in tire construction. The stress changes were estimated by treating the tire as a shell structure. Comparison of calculations using this theory with experimental data taken from thermocouples imbedded in typical aircraft tires showed generally good agreement.

The present report represents an extension of this work to the case of the tire under braking conditions. It is known that brake forces can generate additional tire heat, and in the case of aircraft tires the brake forces are large enough and the energy to be absorbed is so massive, that substantial tire temperature rise may come from the action of the brake alone.

This report presents a theoretical background for the calculation of additional tire heat caused by braking, over and above that due to free rolling. These results must be added to the free rolling temperature rise in order to obtain the total tire temperature under braked rolling conditions. Comparisons are again made between predictions using this theory and data taken on instrumented aircraft tires under braked rolling conditions.

ENERGY ABSORPTION IN A BRAKED WHEEL

The generation of heat in an aircraft tire due to the presence of a braking force is a complex phenomen which involves more than one physical mechanism. For that reason it is appropriate to outline the assumptions used in this study by first considering several simplified cases.

Figure 1 illustrates a rigid rack and pinion operating with frictionless gear teeth, moving to the right at velocity v_0 and under the action of a brake torque, T_0.

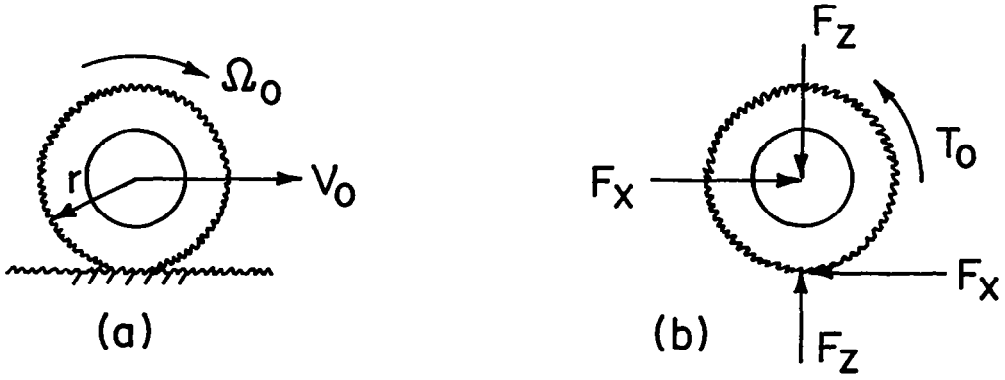

Fig. 1 - Schematic of rack and pinion operating with frictionless gear teeth.

Due to the gear teeth there is no tangential surface slip. Denoting slip velocity by v_s,

$$v_s = 0 = v_0 - r\Omega_0 \quad v_0 = r\Omega_0; \tag{1}$$

In figure 1(b) the forces and couples are shown. The materials are assumed here to be rigid, so that the vertical load $-F_z$ and the resultant of the ground contact vertical pressure distribution $+F_z$ are assumed to be co-linear.

Moment equilibrium requires that

$$F_x r = T_0$$

In the absence of elastic deflection and hysteretic loss in the pinion and rack, all power dissipiated in this model occurs in the brake itself and is given by

$$P = T_0\Omega_0 = F_x v_0 \qquad (2)$$

The energy absorbed from the vehicle ($F_x v_0$) passes entirely into the brake ($T_0\Omega_0$).

Figure 2 shows a rigid wheel but now without the gear teeth of a pinion. Again perfectly rigid materials are presumed, and

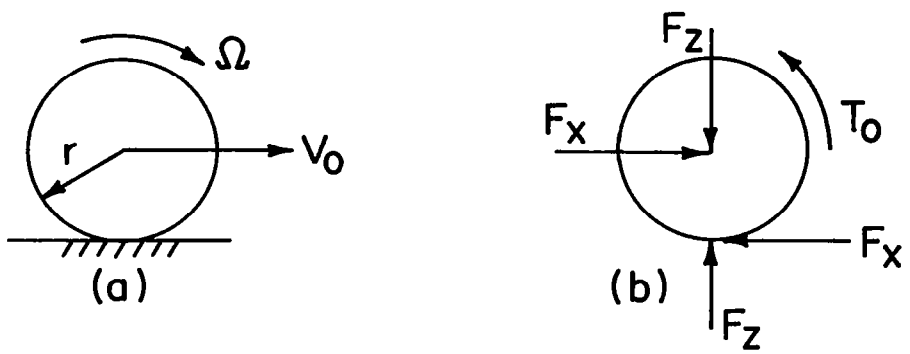

Fig. 2 - Schematic of rigid wheel without gear teeth.

a torque T_0 acts from a brake. In this case however some slip may occur at the interface between the wheel and the plane.

$$v_S \neq 0 = v_0 - r\Omega$$

The total power dissipated is now partitioned between the wheel surface and the brake. The power lost at the brake is

$$P_b = T_0\Omega \qquad (3)$$

and the power loss at the contact surface is

$$P_s = F_x v_s = F_x(v_0 - r\Omega) \tag{4}$$

Note that from figure 2(b), the contact force resultant F_z and the load $-F_z$ are co-linear so that

$$F_x r = T_0$$

and

$$P_s + P_b = F_x v_0 \tag{5}$$

In this case some power is dissipated by the slip at the contact surface, while the remainder goes into the brake.

Next consider a geometry similar to that of fig. 2, but now made of materials which exhibit both elastic and visco-elastic characteristics. This is shown in fig. 3. It represents essentially the case of a real tire.

Here, the deflected wheel exhibits a finite length of contact with the runway surface, and a measureable tire deflection so that the axle height is given by the dimension h.

Similar mechanisms are present here as in the previous two cases. The power absorbed at the tire-runway interface due to slip is given by

$$P_s = F_x v_s \tag{6}$$

and that due to the brake is given by

$$P_b = T_0 \omega \tag{7}$$

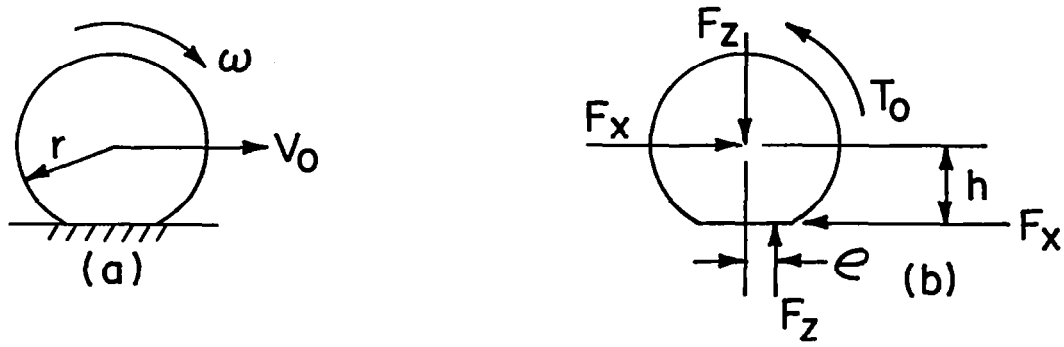

Fig. 3 - Schematic of real tire.

In addition, one new energy loss mechanism is present here, namely the moment $F_z e$ which rotates at angular velocity ω, absorbing power by internal hysteresis of the tire materials, associated with stress cycling of the tire tread and carcass as they rotate. This hysteretic power absorption is

$$P_h = F_z \cdot e \cdot \omega \tag{8}$$

The sum of these three losses must equal the total power absorbed by the vehicle $F_x v_0$ so that

$$F_x v_s + T_0 \omega + F_z \cdot e \cdot \omega = F_x v_0 \tag{9}$$

Figure 3(b) shows that moment equilibrium requires that

$$F_z e + T_0 = F_x h \tag{10}$$

and using this in Eq. (9) results in a simple definition of average slip velocity

$$V_s = v_0 - \omega h \tag{11}$$

Eq. (11) is consistent with the classical definition of slip velocity given in ref. [2] as

$$s = \frac{\omega_0 - \omega}{\omega_0} = 1 - \frac{\omega}{\omega_0} \tag{12}$$

where ω_0 is the unbraked angular velocity of the wheel. Assuming that

$$v_s \simeq v_0 s = v_0\left(1 - \frac{\omega}{\omega_0}\right) \tag{13}$$

and that $h\omega_0 \simeq v_0$, then Eq. (13) reduces to

$$v_s = v_0 - \omega h \tag{14}$$

as in Eq. (11).

The subsequent heating analysis of a braked tire concentrates on the forms of power dissipation just discussed, namely

(a) Power loss due to slip at the tire-runway interface

(b) Power loss due to hystereric losses in the tire materials caused by stress cycling.

Brake temperatures, often many times higher than the tire temperature, can cause heat flow toward the tire, but this heat must usually travel a tortuous conductive path to reach the tire bead region, and during this travel is subject to considerable cooling due to exposed metallic surfaces. This problem is so specific to the individual design features of wheel and brake that it is not included in this analysis.

HEATING DUE TO TIRE SLIP

In order to obtain the slip velocity consider first the angular velocity of the unbraked tire. It may be expressed as

$$\omega_0 = \frac{2\pi V_0}{C_0} \tag{15}$$

where C_0 is the circumference of the tread region of the tire.

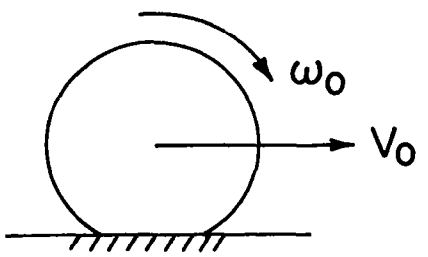

Fig. 4 - Unbraked free rolling tire.

Experimental studies have shown that the length of the contact patch changes very little between free rolling and braked conditions. However, tractive forces in the contact patch cause a longitudinal strain ε. In effect, as far as material passing through the contact patch is concerned, the tire appears to have a greater circumference whose value is $C_0(1 + \varepsilon)$ so that the angular velocity is

$$\omega = \frac{2\pi v_0}{C_0(1+\varepsilon)} \tag{16}$$

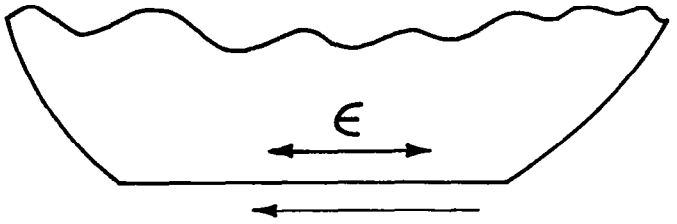

Fig. 5 - Schematic of contact region of braked tire.

The slip due to braking is now

$$s = (1 - \frac{\omega}{\omega_0}) = 1 - (\frac{1}{1+\varepsilon}) \simeq \varepsilon \qquad (17)$$

It is now necessary to estimate the tire carcass strain ε. The vertical load F_z is given approximately by

$$C_1 p_0 A = F_z \qquad (18)$$

where p_0 is the inflation pressure, A the contact area and C_1 is a constant whose value is close to unity.

Let each unit of area in the contact patch be considered as an element elastically restrained in the direction of travel (fore-aft) by a spring of rate K_s, where K_s is the combined elastic effect of the shear in the tread elements plus the elastic deformation of the sidewall structure longitudinally. The average tractive stress is F_x/A, where F_x is the brake force, and the longitudinal strain in the contact patch is

$$\varepsilon = C_2 (F_x/A) \cdot \frac{1}{K_s} = C_3 (F_x/F_z) \frac{P_0}{F_z} \qquad (19a)$$

where C_2 and C_3 are constants and Eq. (18) is utilized.

Most of the spring stiffness K_s is controlled by the elasticity of the tire carcass, which in turn is design-limited by the requirement that it exhibit sufficient strength as a pressure vessel when inflated. Referring to fig. 6, the largest stress is given approximately by

$$\sigma = \frac{P_o a}{t} \tag{19b}$$

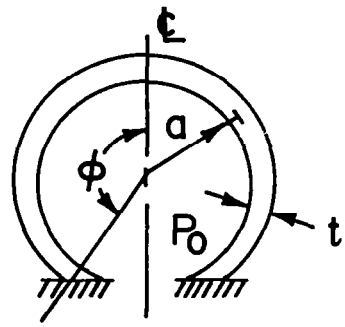

Fig. 6 - Idealized tire section as a pressure vessel.

This stress level is nearly constant among different aircraft tires due to the use of essentially the same structural materials, dictated by other considerations. For this reason it may be assumed that

$$\sigma = C_4 \tag{19c}$$

where C_4 is a constant.

In figure 6, the brake force F_x is applied nearly along the centerline. The distance from the centerline to the bead is proportional to the dimension a in fig. 6, and is given approximately by ϕ a.

By definition

$$K_s = \frac{F'_x}{\delta_x} \tag{20}$$

where F'_x is the brake force per unit length in the contact patch while δ_x is the deflection in the longitudinal direction.

$$\delta_x = \phi \cdot a \cdot \gamma_x \tag{21}$$

where γ_x is the shear strain. But γ_x is given by

$$\gamma_x = \tau_x / G = (\frac{F_x}{t})/G \tag{22}$$

considering an element of unit length running from the center-line to the bead of the tire. Using Eqs. (20), (21), (22),

$$K_s = \frac{F'_x \cdot G \cdot P_0 a}{\phi \cdot a \, F'_x} \cdot C_5 = C_6 P_0 \tag{23}$$

since the shear modulus G of the carcass is nearly constant for all aircraft tires of practical construction.

Substituting into Eq. (19) gives

$$\varepsilon = C_7 (\frac{F_x}{F_z}) \tag{24}$$

or from Eq. (17),

$$C_8 s = F_x / F_z \tag{25}$$

where C_8 is another constant. If the constant C_8 were known, the specification of brake force F_x and vertical force F_z would allow slip s to be calculated.

References [2] and [3] give data on F_x/F_z vs s, and from the initial slope of these curves, prior to the onset of brake

forces sufficient to cause severe tire lock-up and abrasion, it can be estimated that

$$5 \leq C_8 \leq 15 \tag{26}$$

The data is quite consistent over a smaller span than this, with only occasional data points near the lower or upper limits.

Note that due to the assumptions made in this derivation, Eq. (25) may not hold true for conditions far removed from normal operation, such as a tire with extremely low or no inflation pressure.

The mechanical work done per tire revolution is given by

$$\begin{aligned} W &= F_x(\text{Slip distance per revolution}) \\ &= F_x s C_0 = F_x^2 \pi D/(F_z C_8) \end{aligned} \tag{27}$$

This may be converted to the rate of heat release in cal/sec by using appropriate numerical constants to give

$$\dot{Q} = 0.324 F_x^2 v_0/(C_8 F_z) \tag{28}$$

where $\dot{Q}$ = total heat release rate due to tire slip, cal/sec

v_0 = aircraft velocity, feet/second

This quantity of heat is released primarily in the tread region of the tire. It is recognized that contact pressure distributions are not uniform in this region, nor are tractive force distributions. Nevertheless in the absence of a much more detailed analysis of the contact patch area it will be assumed that this heat is uniformly distributed throughout the

total tread volume. The total volume is chosen since in most aircraft tires the tread depth is quite small, and secondly there is some hysteretic loss in this relatively thin tread region.

The average rate of heat generation in the tread region is

$$\dot{q} = (0.0063F_x^2 v_0)/(C_8 F_z Dwt) \text{ cal/cm}^3\text{sec} \qquad (29)$$

where D = tire diameter, in.

w = tread width, in.

t = tread thickness, in.

This value of heat generation will be assigned on a uniform basis to the tread of the tire.

Note that the rate of heat generation is proportional to the square of the brake force F_x.

HEATING DUE TO BRAKING STRESSES

Reference [1] calculated temperature rise in a free rolling tire by using the concept of stress cycling between extreme points on the tire, shown as points A and B in fig. 7.

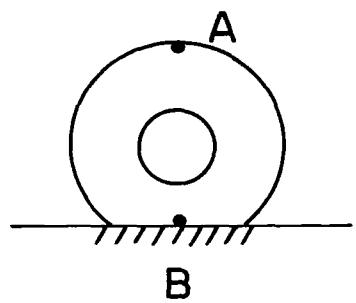

Fig. 7 - Extreme points A and B for calculating stresses.

During the process of rolling with a brake force acting, it will be assumed that the stresses at point A of the tire are unaffected. However, the stresses at point B must be modified to account for the tractive force F_x and the influence it has on the membrane stresses in the tire carcass. It is assumed that no change in bending stress occurs.

Assume the contact patch to be rectangle of length ℓ and width b, acted upon by a brake force F_x tangent to the carcass and kept in equilibrium by cord tension increments at the rear and sides of the contact patch, generating tensile forces. Only one-half of the cords along the sides are effective, since cords in compression are assumed to carry no load. A bias construction is assumed. This is illustrated in fig. 8.

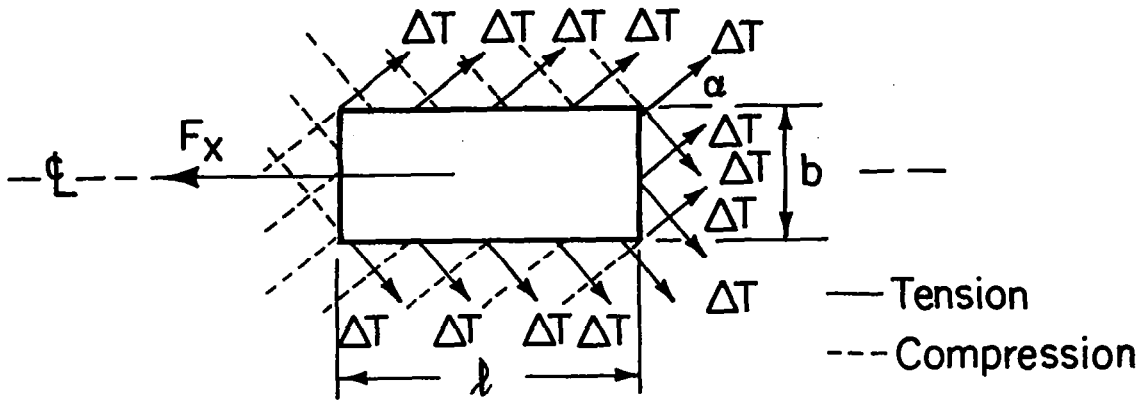

Fig. 8 - Idealized contact patch illustrating distribution of cord tensions and compression.

The average cord tension change may be computed from equilibrium of the contact region.

$$F_x = 2\left(\frac{n}{2}\Delta T \ell \cos\alpha\right)(\bar{e}\sin\alpha) + bn\Delta T\cos\alpha(\bar{e}\cos\alpha)$$

$$= \Delta T n \bar{e}(\ell \sin\alpha\cos\alpha + b\cos^2\alpha) \qquad (30)$$

where n = number of plies

α = cord angle measured from the centerline

$\bar{e}$ = cord end count (cords per unit length)

ℓ = contact patch length

b = contact patch width

The geometric details are shown in fig. 9.

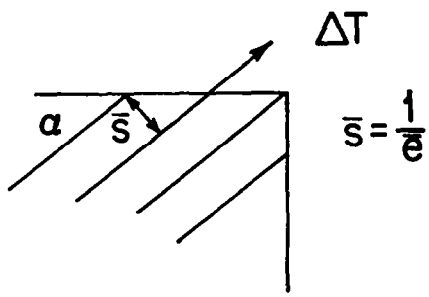

Fig. 9 - Geometric details in contact patch.

In Ref. [1] the membrane forces in the tire were described by N_ϕ and N_θ, the latter being the circumferential direction.

For a small element of bias construction such as shown in fig. 10, the membrane forces may be related to the cord tensions by the relations

$$\Delta N_\theta \left(\frac{1}{\bar{e}\cos\alpha}\right) = n\Delta T\cos\alpha \qquad \text{or,}$$

$$\Delta N_\theta = \Delta T \cdot n \cdot \bar{e} \cdot \cos^2\alpha \tag{31}$$

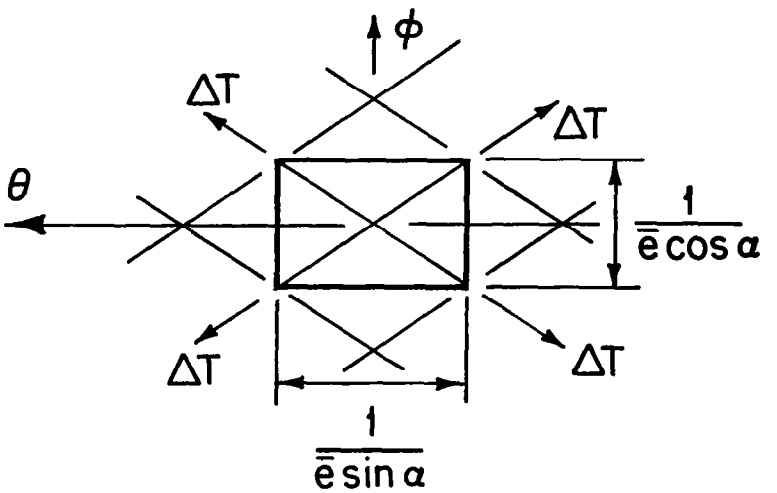

Fig. 10 - Small element in contact region illustrating relations between membrane forces and cord tensions.

Similarly, $\Delta N_\phi \left(\frac{1}{\bar{e}\sin\alpha}\right) = n\Delta T\sin\alpha$ or,

$$\Delta N_\phi = \Delta T \cdot n \cdot \bar{e} \cdot \sin^2\alpha \tag{32}$$

The perturbations in N_θ and N_ϕ caused by the brake force can be obtained by using the additional cord tension which that brake force generates, given in Eq. (30), in Eqs. (31) and (32)

$$\Delta N_\theta = F_x \cos^2\alpha / (\ell \sin\alpha\cos\alpha + b\cos^2\alpha) \tag{33}$$

$$\Delta N_\theta = F_x \sin^2\alpha / (\ell \sin\alpha\cos\alpha + b\cos^2\alpha) \tag{34}$$

These membrane forces must be added to those found in Ref. [1] for free rolling conditions, but only near the contact patch. Away from the contact area these forces diffuse and decay rapidly, due to the geometry of the cord structure.

MEASURED AND CALCULATED RESULTS

Two separate test programs were conducted to provide test data on the temperature distributions in aircraft tires during braking operations. The results of these tests provided insight into the general phenomena associated with a braked rolling tire. Furthermore these programs provided a great deal of data which could be used to evaluate the validity of the analytical model described above.

Two tires, each of different sizes, were used in these test programs. These were 22 x 5.5, 12 PR and 40 x 14, 28 PR aircraft tires. Each tire was instrumented with an extensive set of thermocouples.

The installation of the thermocouples began by carefully laying out the desired locations on the surface of each tire. An illustration of these locations for each of the two tire sizes is shown in figure 11. It can be seen in this figure that a good picture of the tire temperature distribution can be obtained with these locations, since they span the thickness of the carcass as well as the meridian.

Small holes were drilled for implanting all interior thermocuples. The tires were then shipped to a commerical re-treader where the treads were buffed off and the thermocuples in the tread region installed just prior to the retreading.

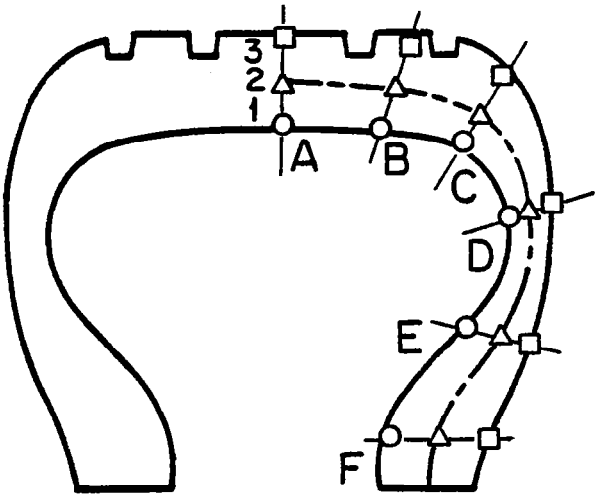

22 x 5.5 12 PR

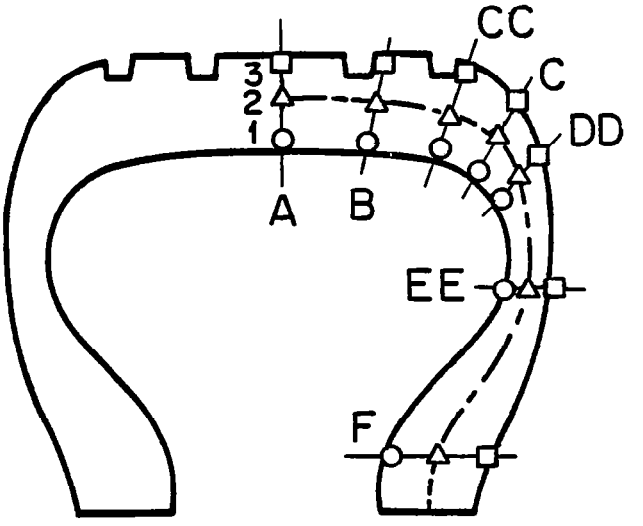

40 x 14 28 PR

Fig. 11 - Location of thermocouples in test tires used in braked rolling thermal study.

After the retreading process the tires were returned to the laboratory where the remaining thermocouples were inserted in their proper locations and sealed with a hot patch process.

A 40 x 14, 28 PR tire fully instrumented with a set of thermocouples, mounted on an appropriate wheel, and wired for recording all thermocouples, is illustrated in figure 12.

The first of the test programs was carried out by the Impact Dynamics Branch, Langley Research Center, National Aeronautics and Space Administration, Hampton, Virginia. This work was done at the Wallops Flight Center using a truck which has been modified by adding a rear-mounted tire test fixture. Tire loads were applied through a pneumatic cylinder. The output from the thermocouples, as collected through slip rings, was routed to an automatic data logger. An instrumented trailing wheel was used to provide an accurate measurement of vehicle speed and distance traveled.

These NASA tests consisted of temperature-time profiles for a variety of operating conditions. The major emphasis in these tests was to ascertain the influence of variable brake force on the temperature distribution in a braked, rolling tire. A list of the NASA test operating conditions is shown in Table 1. All of these tests were carried out using 22 x 5.5, 12 PR tires.

The second test program was carried out by the University of Michigan on the automated 120-inch diameter dynamometer at the Air Force Flight Dynamics Laboratory, Wright-Patterson Air

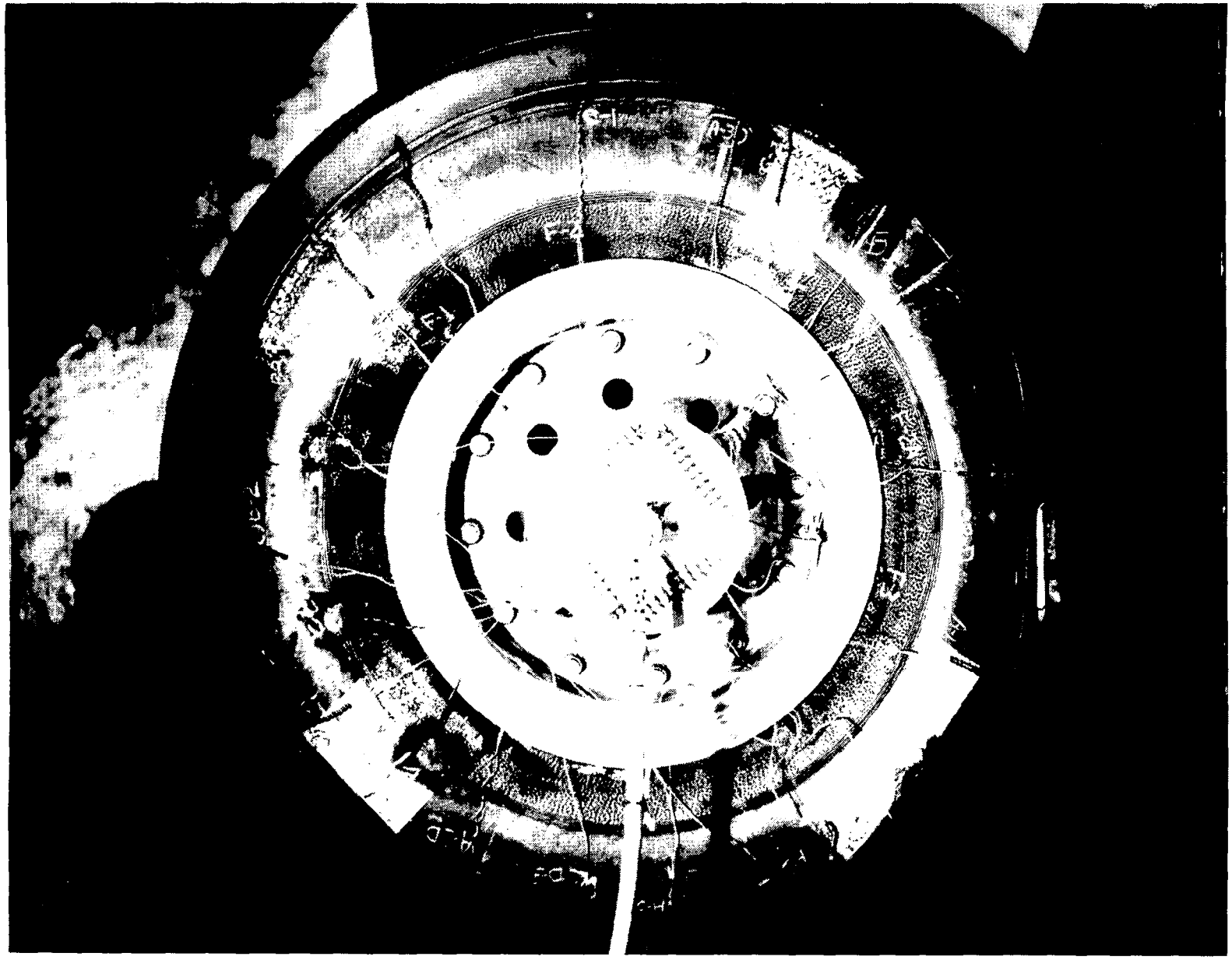

Fig. 12 - Instrumented 40 x 14, 28 PR tire loaded against the Air Force Flight Dynamics Laboratory 120-inch diameter dynamometer.

Table 1

Operating Conditions NASA Langley Tests

22 x 5.5, 12 PR tires

Load lbs	Deflection in.	Deflection %	Pressure psi	Brake Force lbs.	Speed MPH
4100	1.30	26.0	97	0	20
4100	1.30	26.0	97	1164	20
4100	1.30	26.0	97	2056	20
4200	1.30	26.0	97	2649	20
4200	1.08	21.6	125	1998	20
4200	1.52	30.4	73	2483	20

Table 2

Operating Conditions - University of Michigan Tests

40 x 14, 28 PR tires

Load lbs	Deflection in.	Deflection %	Pressure psi	Brake Force lbs.	Speed MPH
24000	2.67	22.4	226	0	20
24000	2.67	22.4	226	5545	20
22500	2.67	22.4	206	5549	20
30500	3.20	26.9	226	5540	20
26800	2.67	22.4	246	5536	20
39500	4.00	33.6	226	5662	20

Force Base. This dynamometer consists of a cantilevered wheel mounting fixture which is hydraulically loaded against the driven dynamometer wheel. The radial load on the tire was measured by strain gage beams in the mounting fixture. The thermocouple signals were routed through slip rings and recorded in an exterior data logger.

The University of Michigan tests also consisted of temperature-time profile measurements for a variety of operating conditions. The brake torque capacity was limited in these tests, and it was not possible to study the influence of variable brake force on tire temperature distributions. However, other effects could be studied more easily than with the NASA test equipment. Thus the major emphasis in the University of Michigan work was to examine the influence of inflation pressure and vertical deflection on the internal temperature distribution. A list of the University of Michigan test operating conditions is presented in Table 2. All of these tests were carried out using 40 x 14, 28 PR tires.

From the results of the two test programs it was possible to examine the effects of four major operating parameters, load, deflection, pressure and brake force on the temperature distribution in a braked rolling aircraft tire.

The analytical model described previously was used to calculate temperature profile for aircraft tires under braking operations. The input operating parameters used in the computer program were the same as those described in the test matrices of Tables 1 and 2.

The first set of comparisons between calculated and measured temperature profiles is shown in figures 13 - 19, and figures 20 - 25. These are composite plots of all of the calculated and measured temperature values of the two sets of test tires, as a function of time, for a speed of twenty miles per hour and at various operating conditions. The ordinate of these plots is the temperature rise above the initial temperature value. The abscissa in these plots is the thermocouple location noted in figure 11.

Figure 13 illustrates a typical comparison of measured and calculated values under free rolling conditions for a 40 x 14, 28 PR tire, while figure 14 illustrates similar comparisons for the same tire and operating conditions with an applied brake force. As can be seen, there is generally good agreement between calculated and measured results for both the braked and free rolling conditions. It is also noted from these two figures that the major effects due to braking take place in the contact region of the tire. This is more clearly illustrated in figure 15 where the change in temperature rise between the braked condition and the free rolling condition is plotted throughout the cross section. Here it is clearly seen that nearly all of the temperature rise between braked and free rolling operations is in the contact region. This is verified both experimentally and analytically.

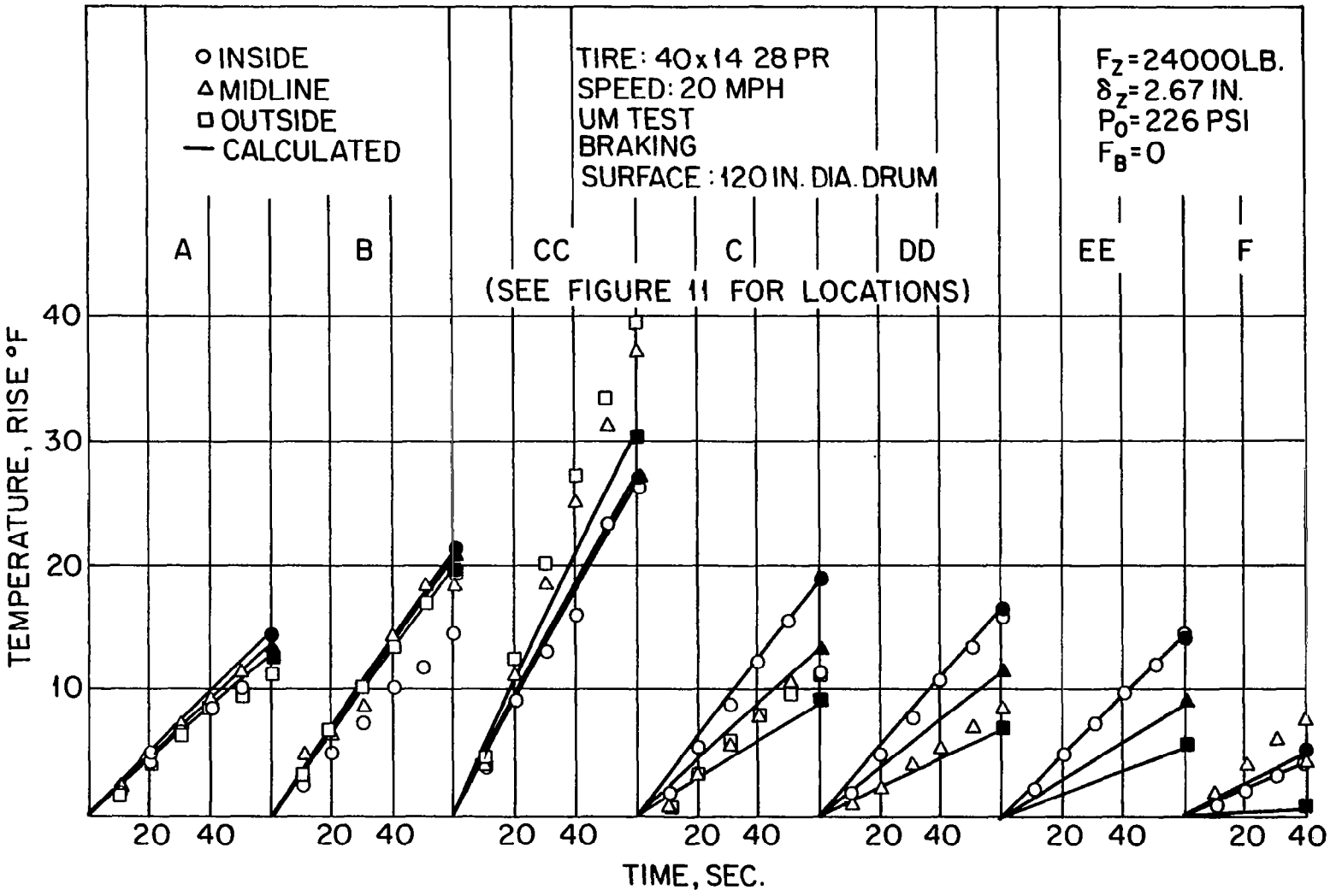

Fig. 13 Measured and Calculated Tire Temperature Profiles for a Free Rolling Tire

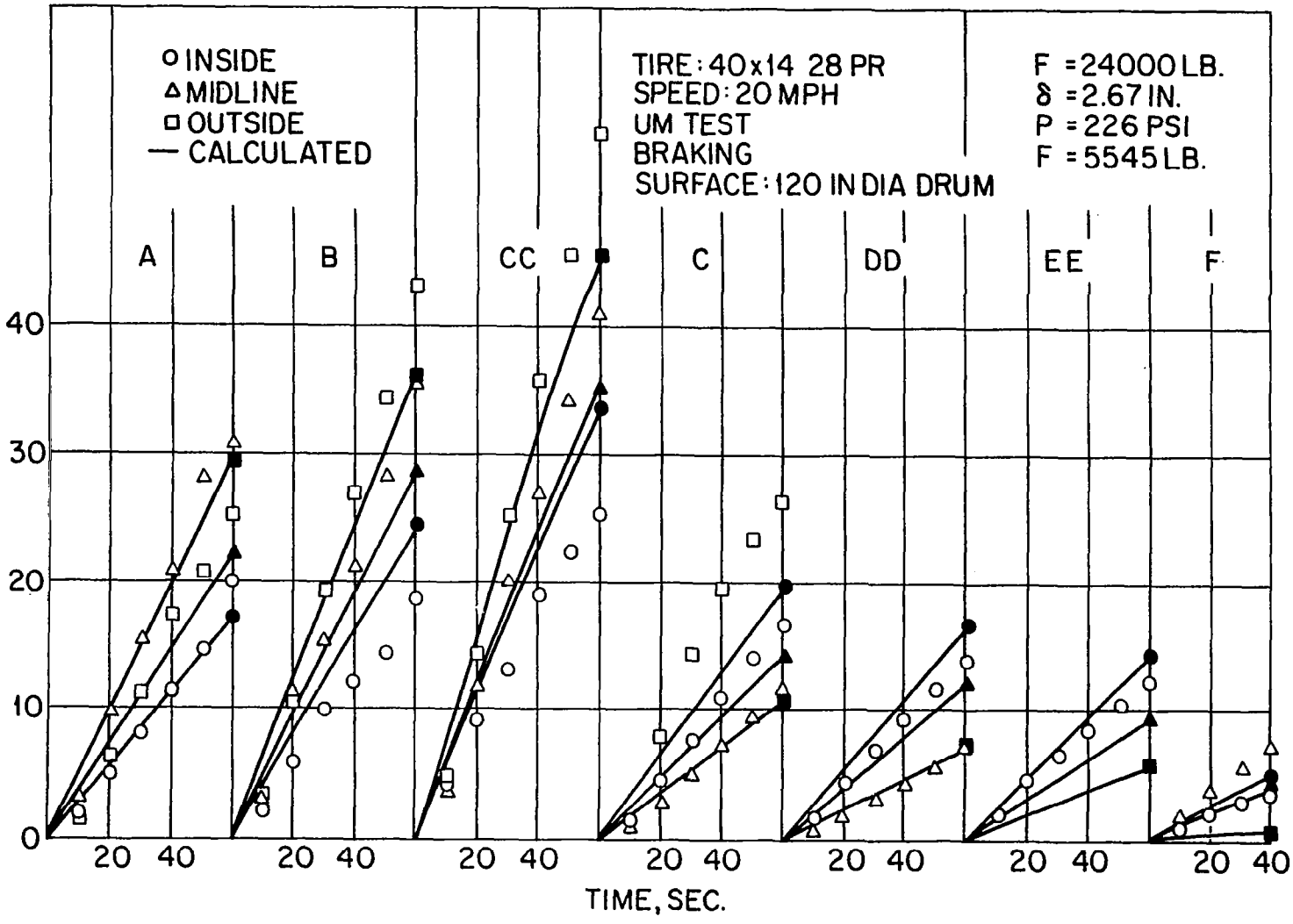

Fig. 14 Measured and Calculated Tire Temperature Profiles for a Braked Tire

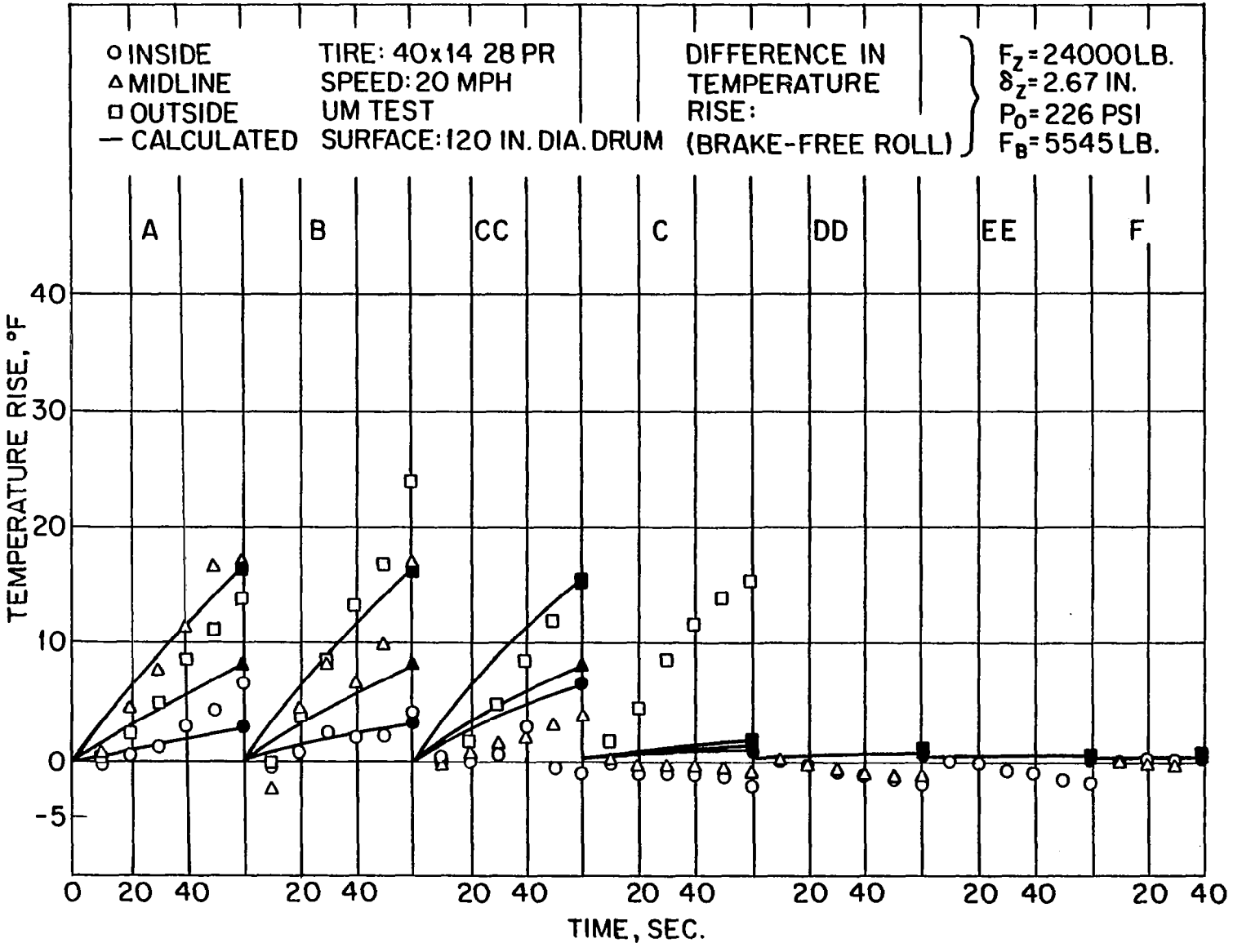

Fig. 15 Calculated and Measured Temperature Change - Free Rolling to Braked Rolling

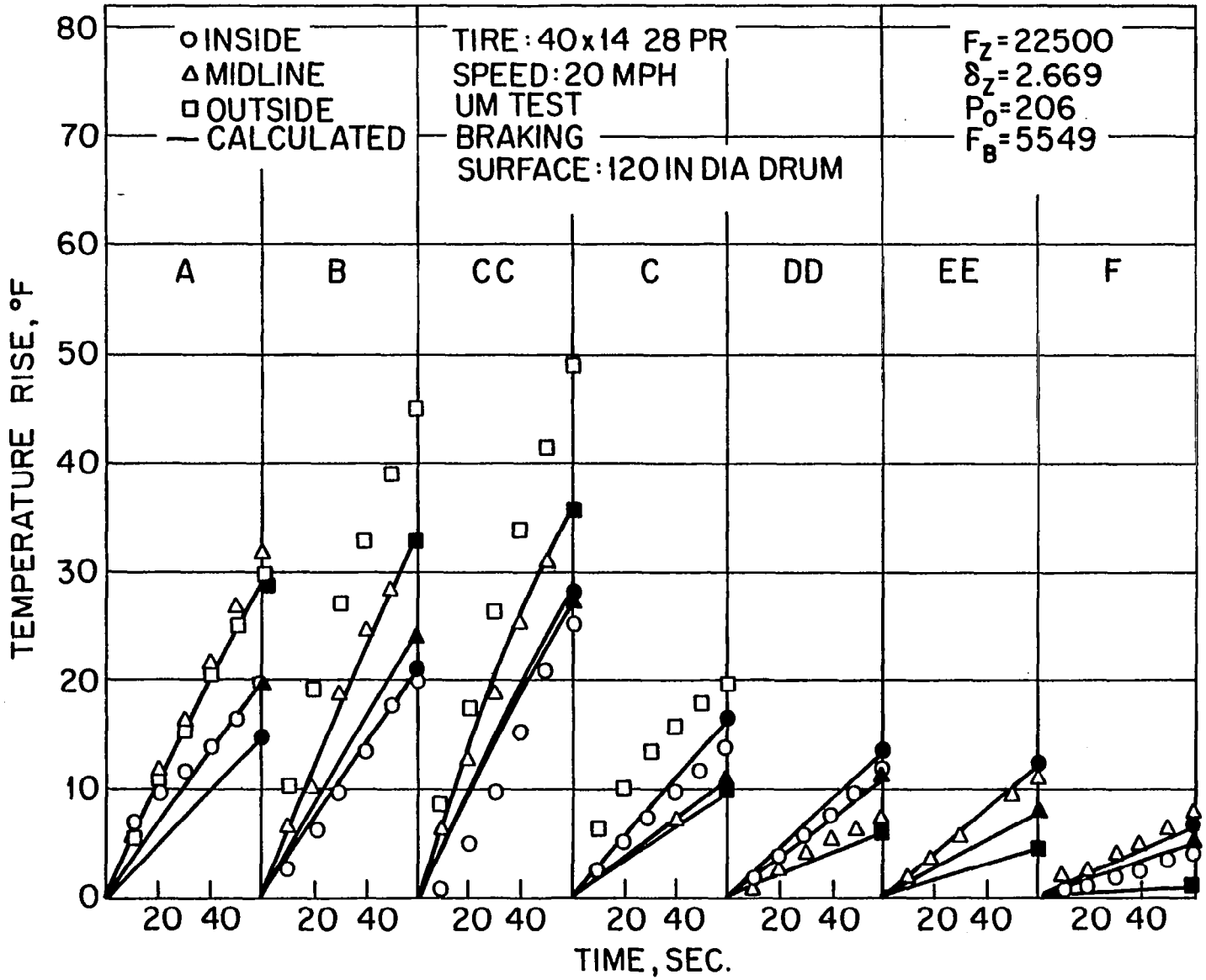

Fig. 16 Measured and Calculated Tire Temperature Profiles for a Braked Tire

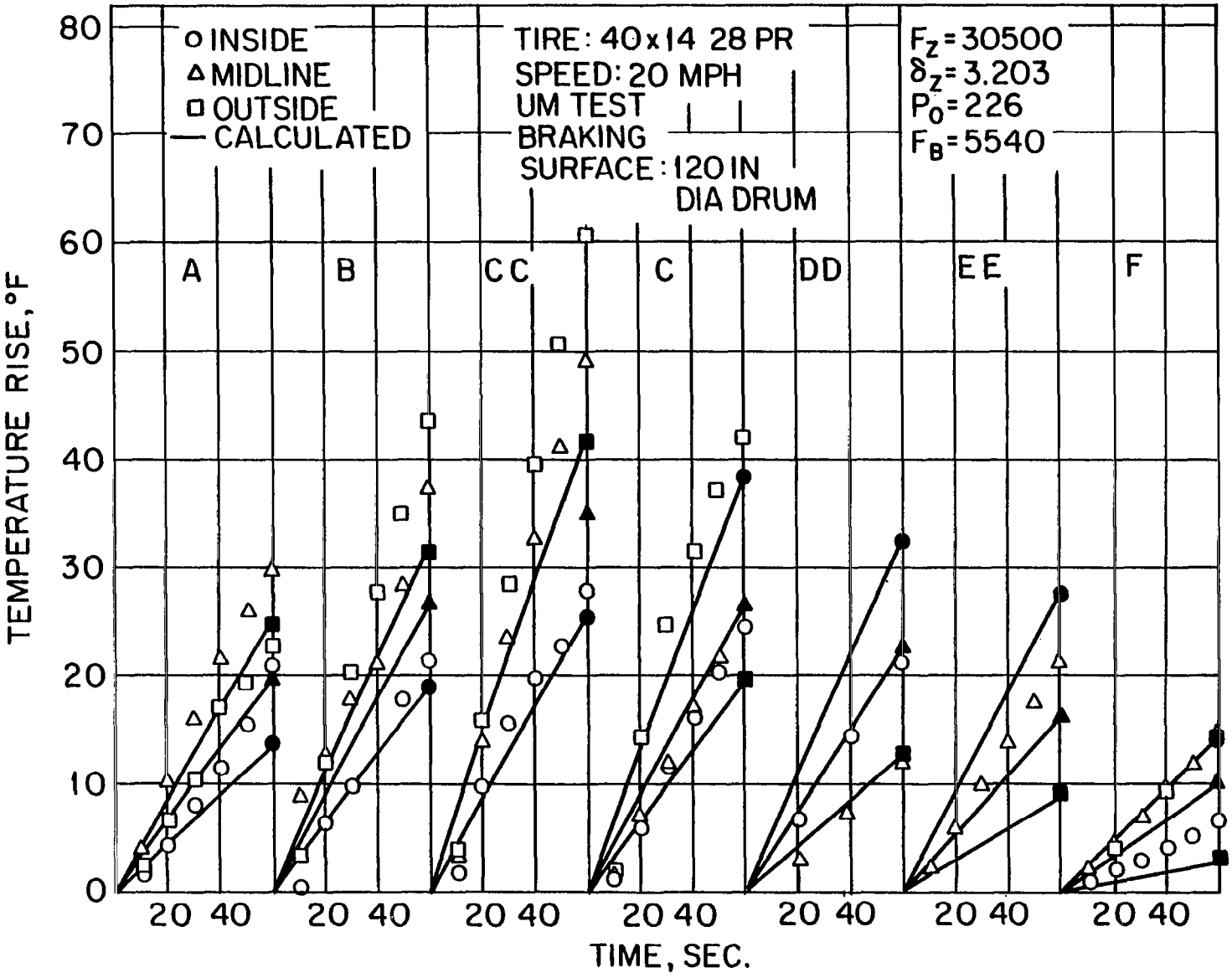

Fig. 17 Measured and Calculated Tire Temperature Profiles for a Braked Tire

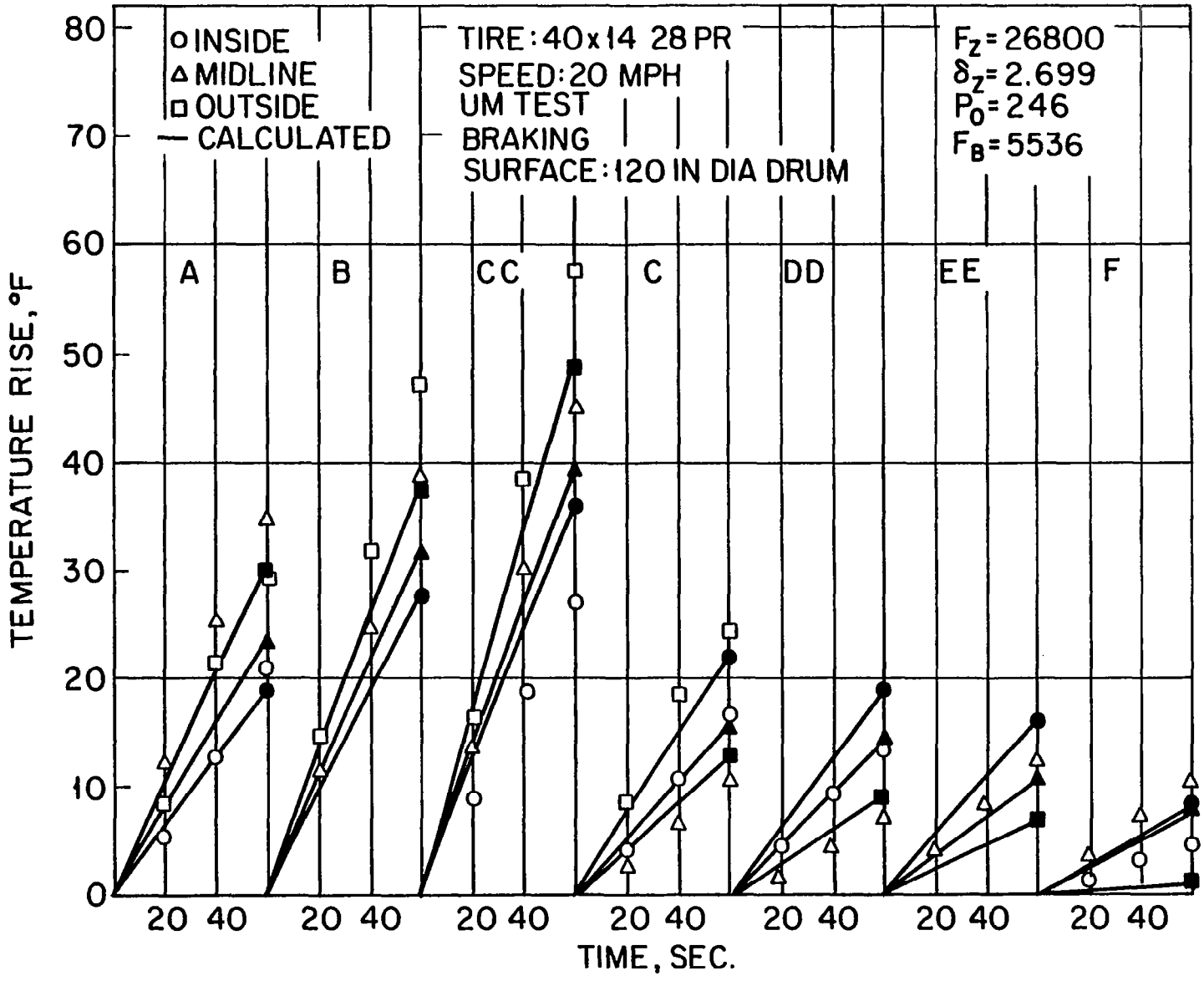

Fig. 18 Measured and Calculated Tire Temperature Profiles for a Braked Tire

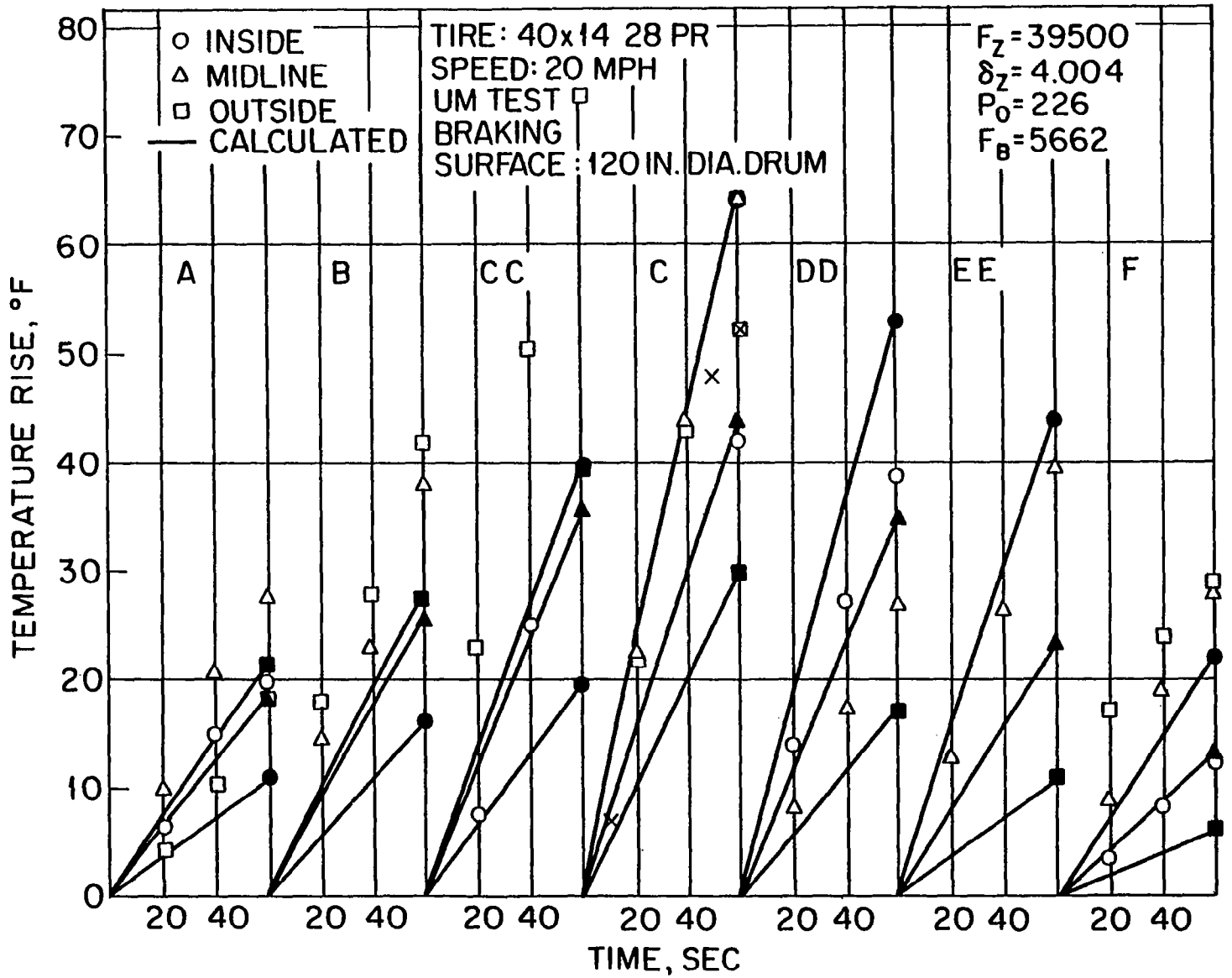

Fig. 19 Measured and Calculated Tire Temperature Profiles for a Braked Tire

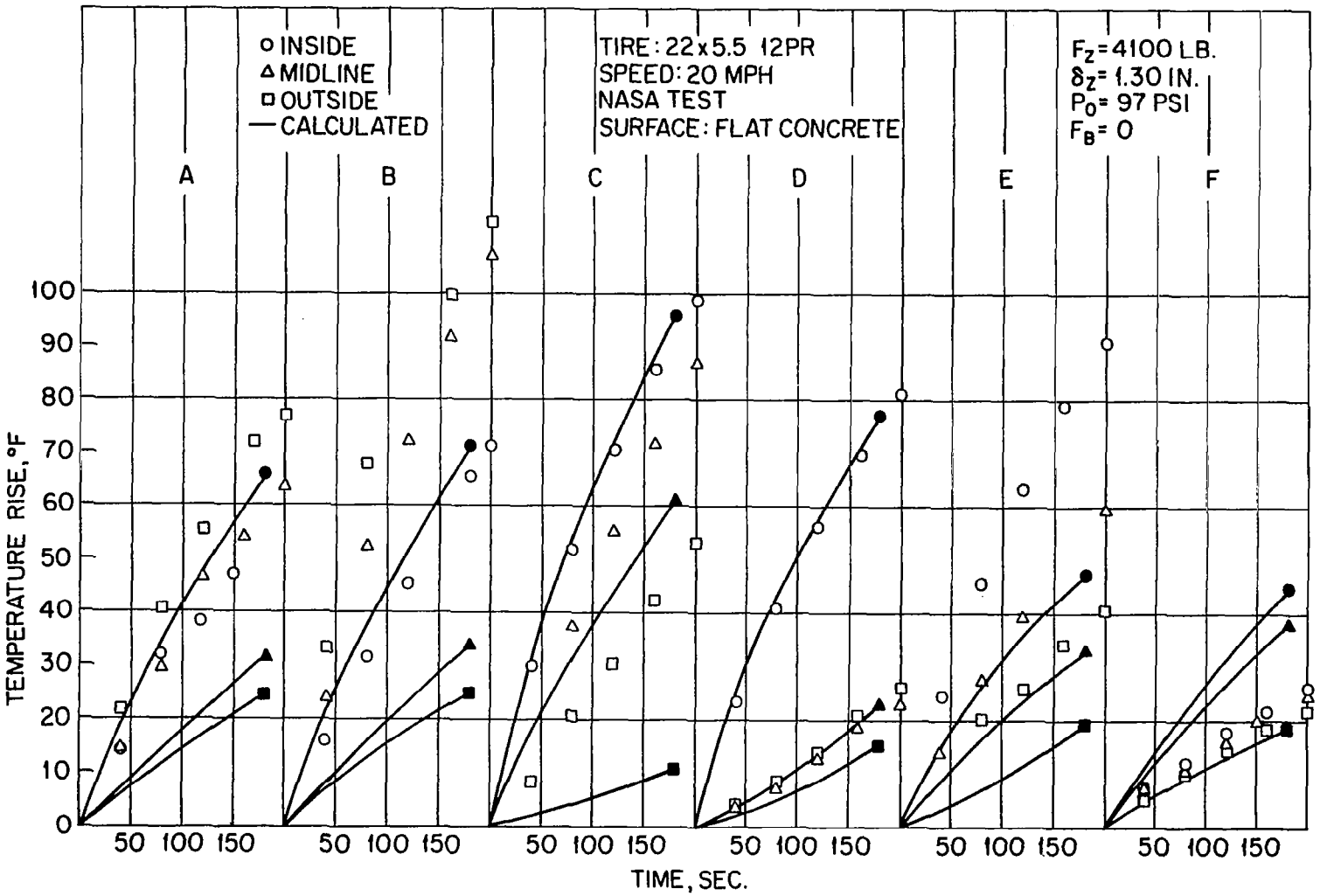

Fig. 20 Measured and Calculated Tire Temperature Profiles for a Braked Tire

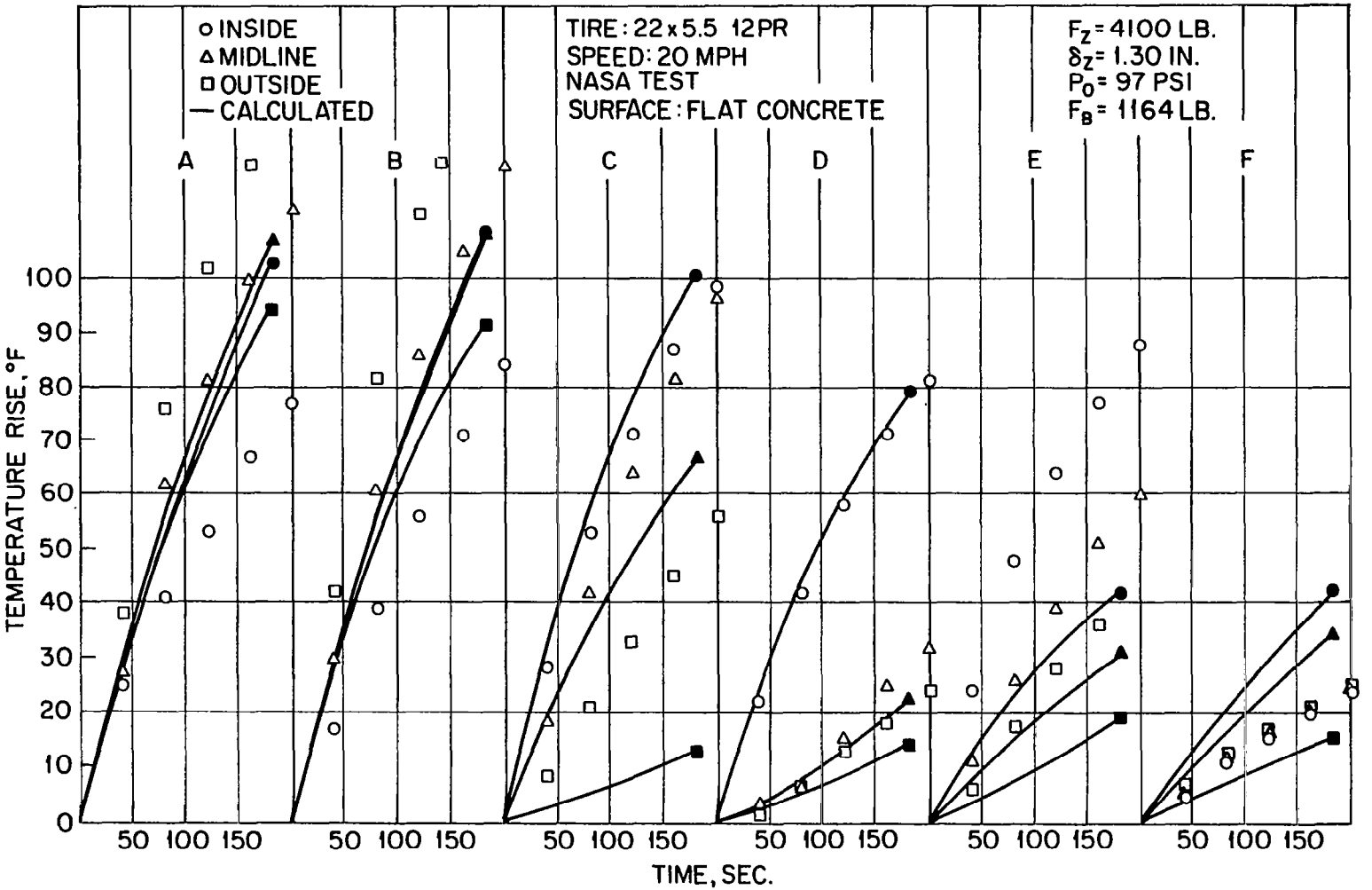

Fig. 21 Measured and Calculated Tire Temperature Profiles for a Braked Tire

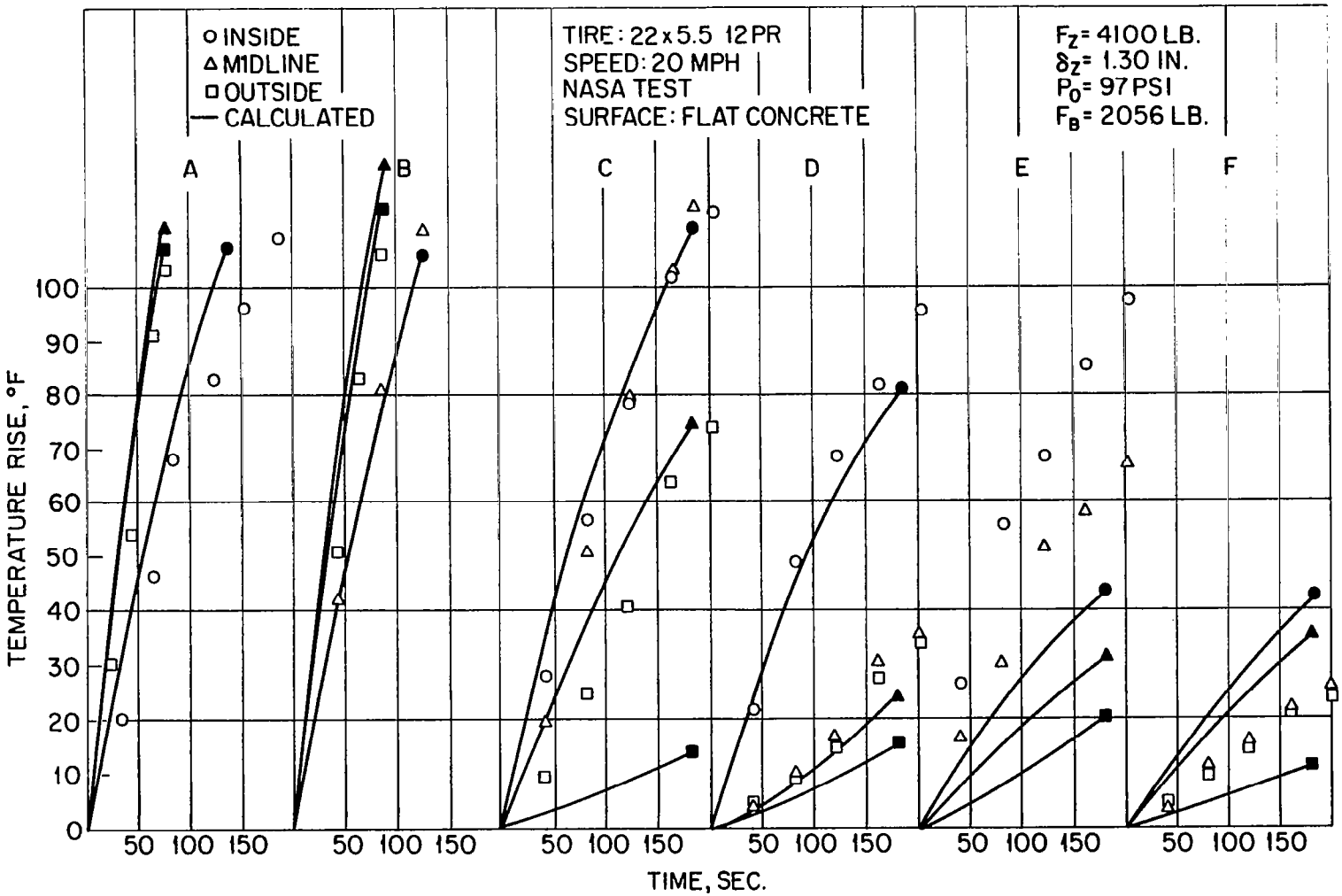

Fig. 22 Measured and Calculated Tire Temperature Profiles for a Braked Tire

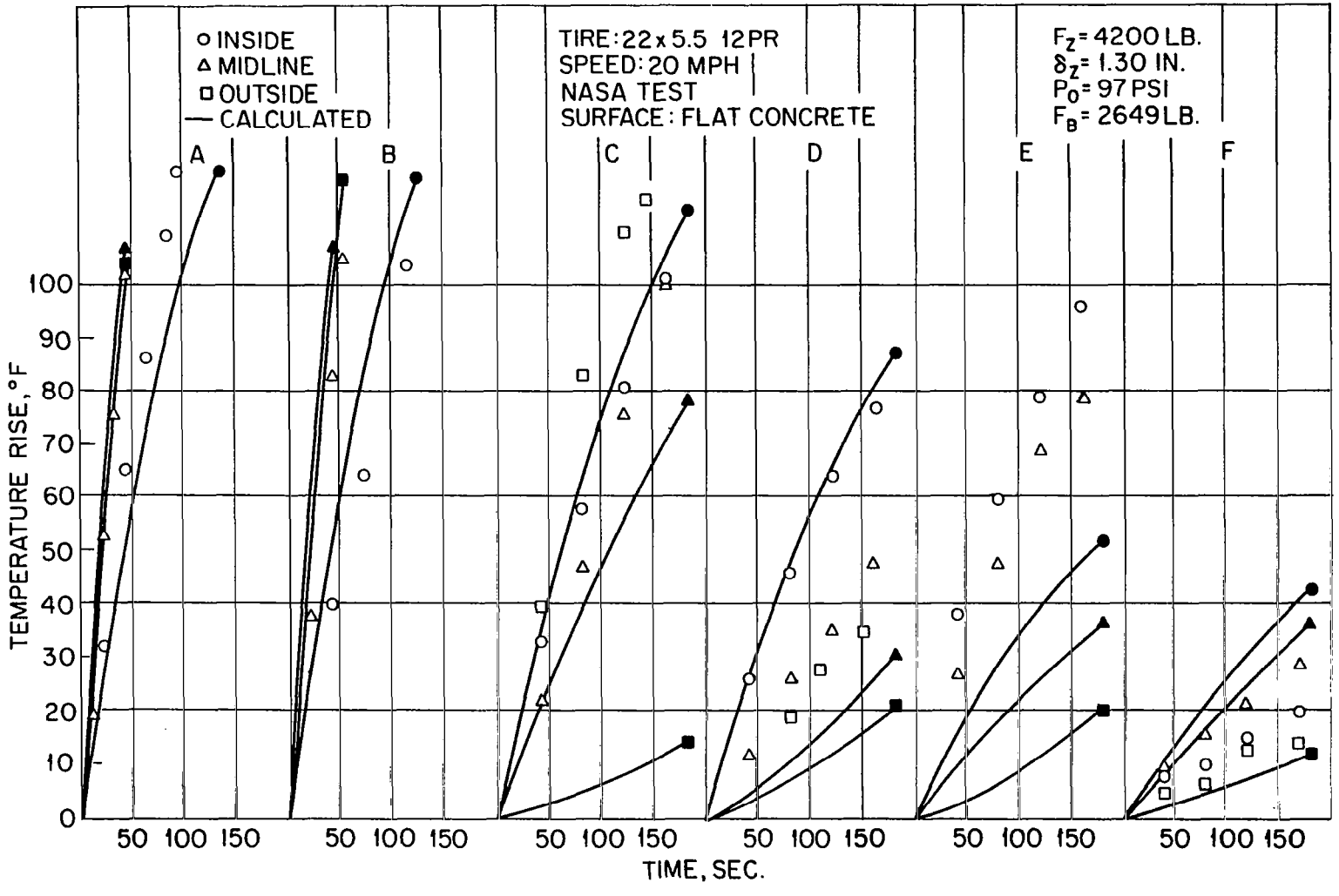

Fig. 23 Measured and Calculated Tire Temperature Profiles for a Braked Tire

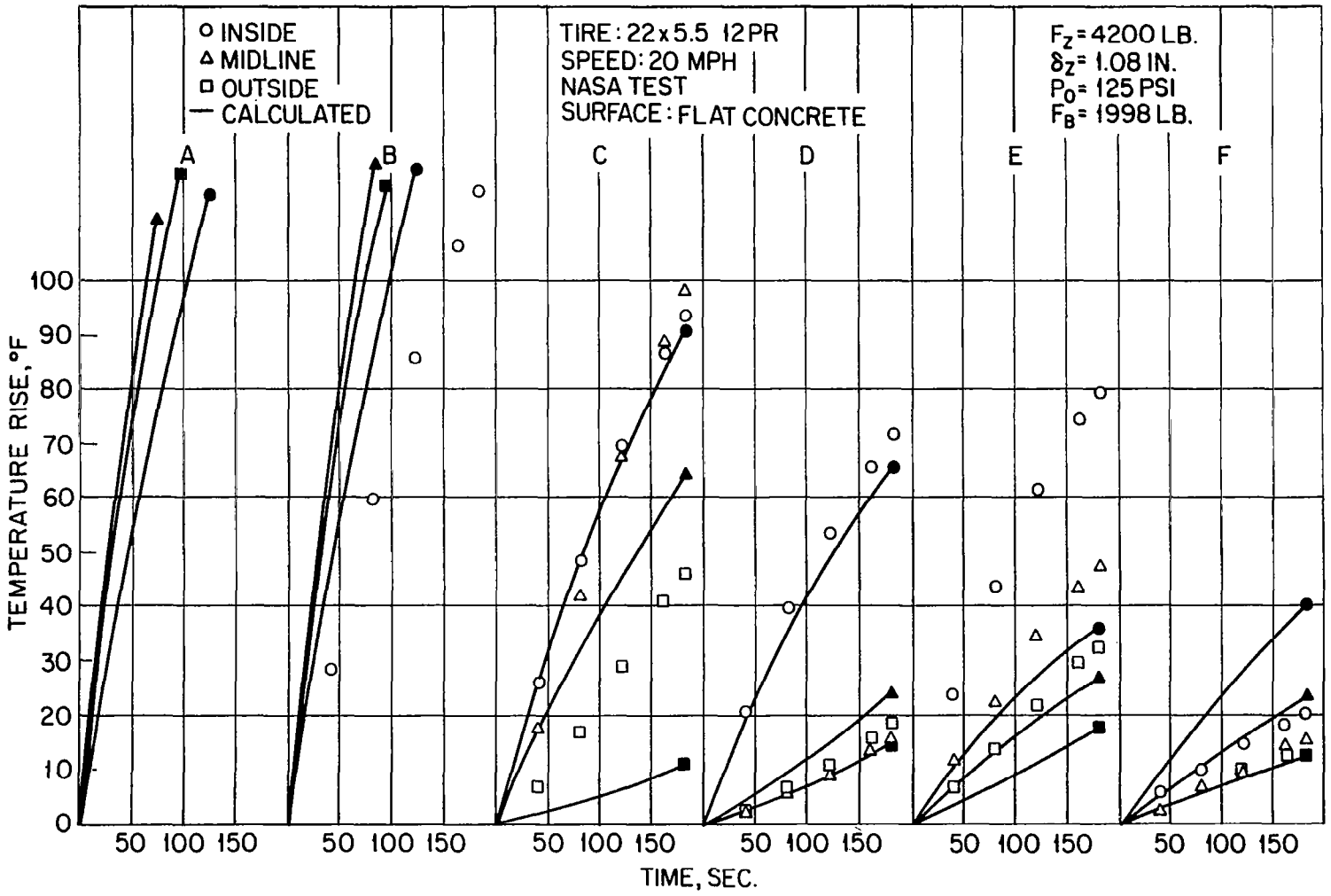

Fig. 24 Measured and Calculated Tire Temperature Profiles for a Braked Tire

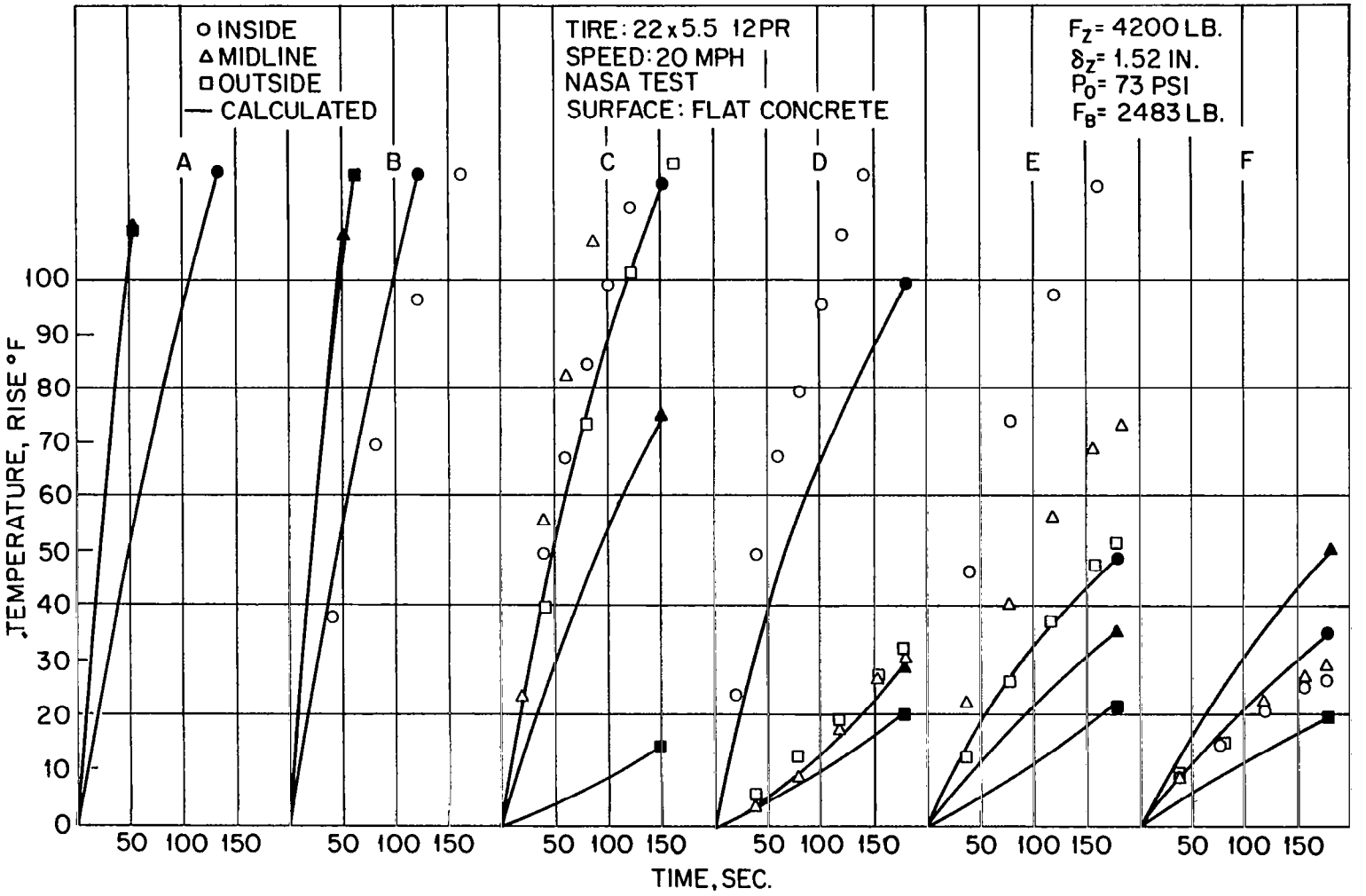

Fig. 25 Measured and Calculated Tire Temperature Profiles for a Braked Tire

All calculated and measured results are reasonably comparable except for the outside location of Section C (see fig. 11) which is near the surface just out of contact in the free rolling tire. However, when the tire is braked it sinks just enough to cause this point on the tire to come into contact with the road surface, and thus to experience a greater rise in temperature during braking. The analytical model does not account for the sinkage during braking, and thus the calculated results in this region are not in good agreement with the measured values.

Figures 16 - 18 are plots of calculated and measured temperature profiles of the 40 x 14, 28 PR tires for the other operating conditions in Table 2. The agreement between the calculated and measured results remains good except for the outside region of Section C.

Figures 20 - 25 are similar plots for the 22 x 5.5, 12 PR tires used in the NASA test program described in Table 1. Again there is generally good agreement between calculated and measured results although there is poor agreement in the lower sidewall region. This poor agreement stems from the poor correlation with the free rolling effects rather than from the braking effects.

The effect of inflation pressure on temperature distribution in the tire carcass is illustrated in figure 26. In this plot the ordinate is the temperature rise above the initial temperature and the abscissa is the meridianal location of the temperature measurement. These plots are from data and calculations of the 40 x 14, 28 PR tire at a time of 60 seconds, a speed of 20 miles

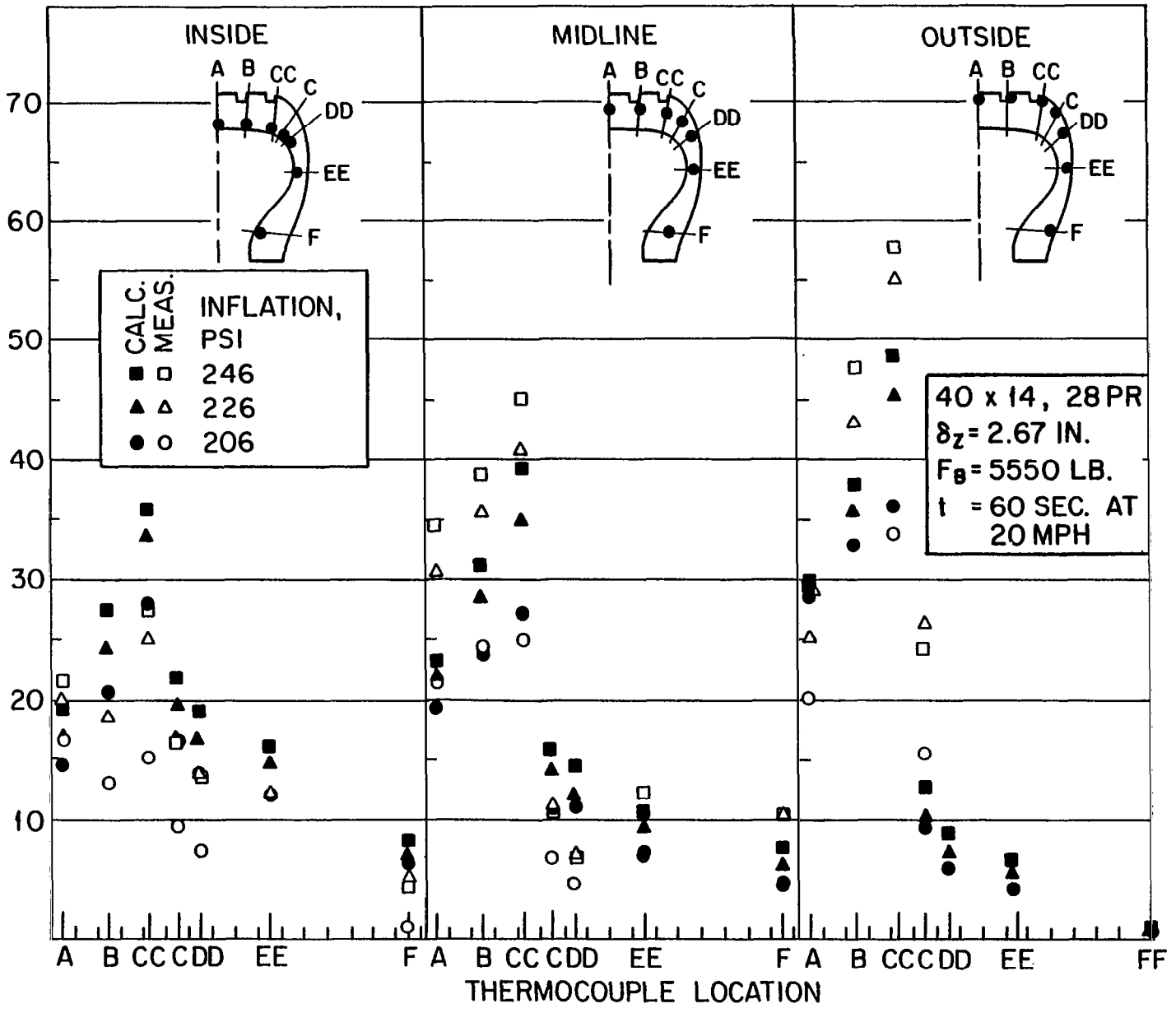

Fig. 26 Influence of Inflation Pressure on Temperature Rise

per hour, a vertical deflection of 2.67 inches, and a constant brake force of 5550 pounds. As can be seen, the temperature rise increases with increasing pressure from the crown to the bead. The change is relatively uniform throughout the thickness as well as around the meridian. The experimental and calculated results are in relatively good agreement.

The effect of brake force on temperature distribution is illustrated in figure 27. Again the ordinate is the rise in temperature above the initial temperature and the abscissa is the meridional location. These plots are from data and calculations of the 22 x 5.5, 12 PR tires at a time of 60 seconds, a speed of 20 miles per hour, a vertical deflection of 1.30 inches and an inflation pressure of 97 psi. As was noted previously, the major effect due to braking is found in the contact region where there is a significant increase in the temperature rise as the brake force in increased. The remainder of the cross section is affected very little by the brake force. Again there is generally good agreement between the calculated and measured values.

The effect of vertical deflection on temperature distribution is illustrated in figure 28. The ordinate is again the rise in temperature above the initial temperature and the abscissa is the meridional location. These plots are from data and calculations of the 40 x 14, 28 PR tires at a time of 60 seconds, a speed of 20 miles per hour, an inflation pressure of 226 pounds per square inch and a constant brake force of 5550 pounds. As

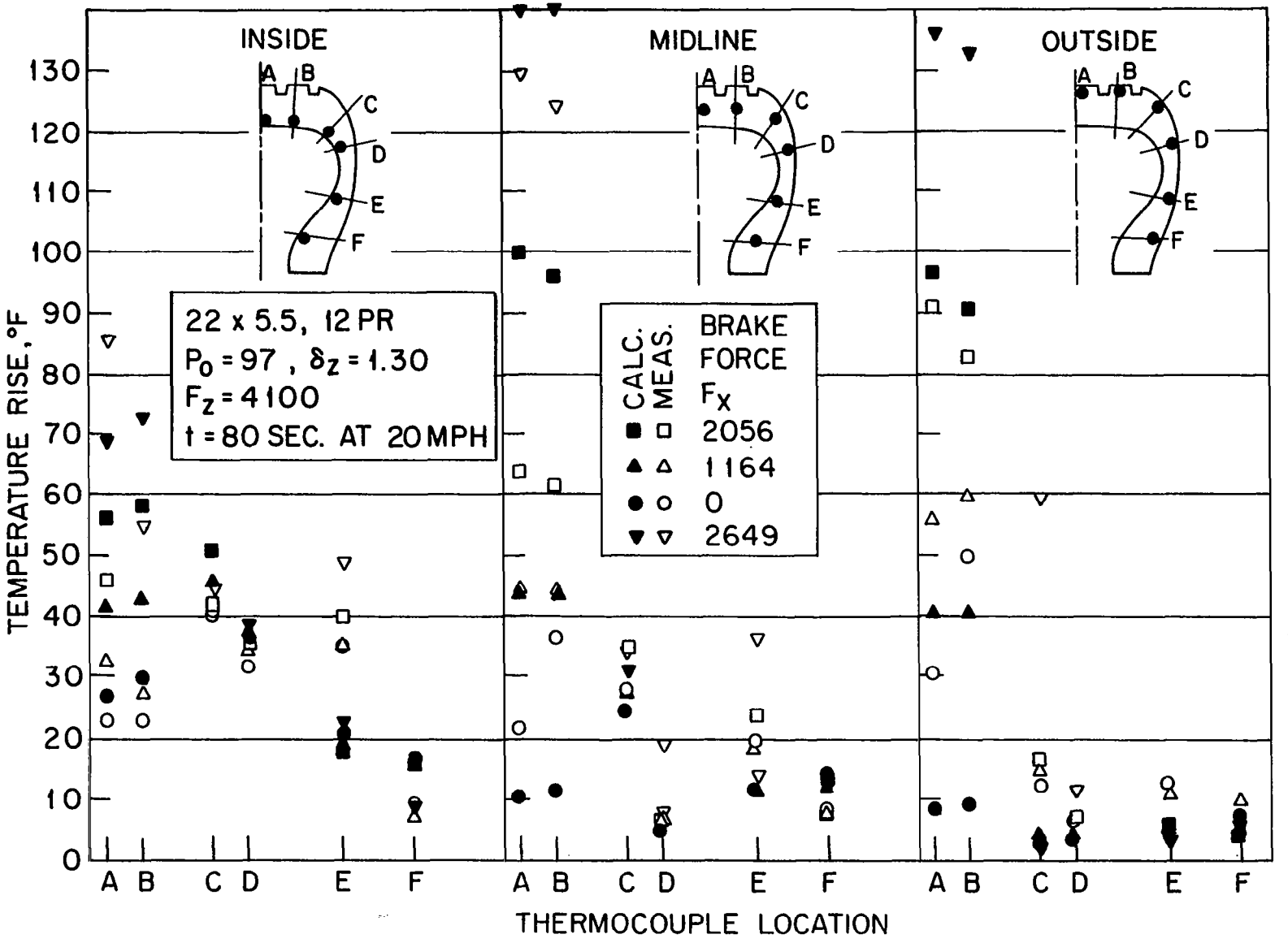

Fig. 27 Influence of Brake Force on Temperature Rise

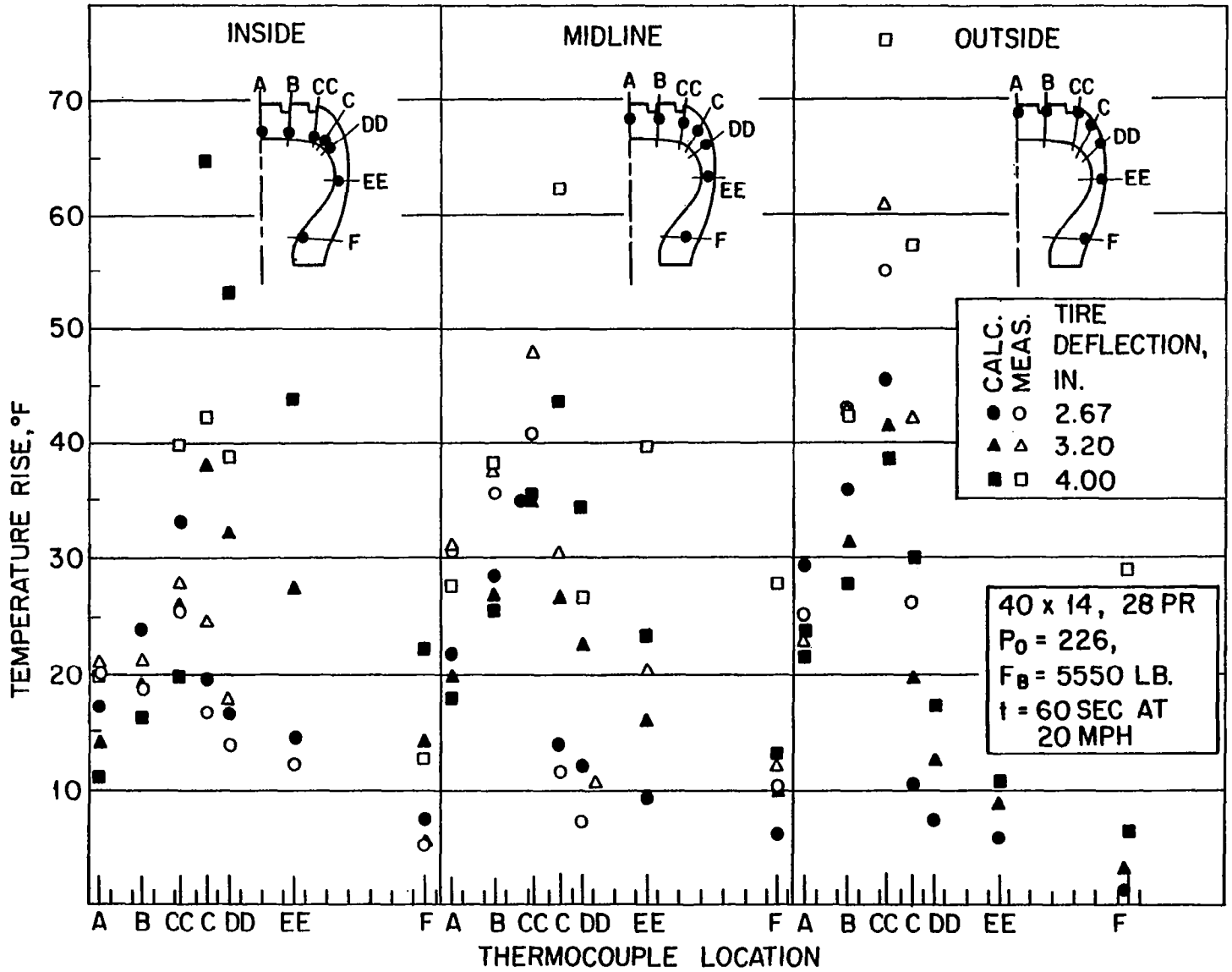

Fig. 28 Influence of Tire Deflection on Temperature Rise

expected the higher temperature rises occur with greater deflections. The agreement between calculated and measured values is not especially good. This is probably due to the difficulty in computing the bending stiffness of cord-rubber composites accurately.

A more detailed comparison of calculated and measured results for a specific test is illustrated in figures 29 - 32 where the measured values are plotted along with the calculated values on a time base. These plots are similar to those shown in figures 20 - 25 except that the scale has been expanded and only one location has been illustrated in each figure. For instance, figure 29 shows the results of an individual test run at the center of the contact region, both for the inside and outside surface locations. It is worth noting that the plots for the outer surface appear parallel but off-set by some fixed value. This was a common occurrence which often resulted from an inability to establish the absolute initial value of an individual thermocouple reading. Figures 30, 31, and 32 show similar detailed plots for other regions of the tire for the same test run illustrated in figure 29. In all of these plots the correlation between measured and calculated curves are reasonably good with the exception of the region in the outside of the shoulder which is not in contact with the road surface during free roll. As was discussed previously, this latter correlation is poor because the analytical model does not account

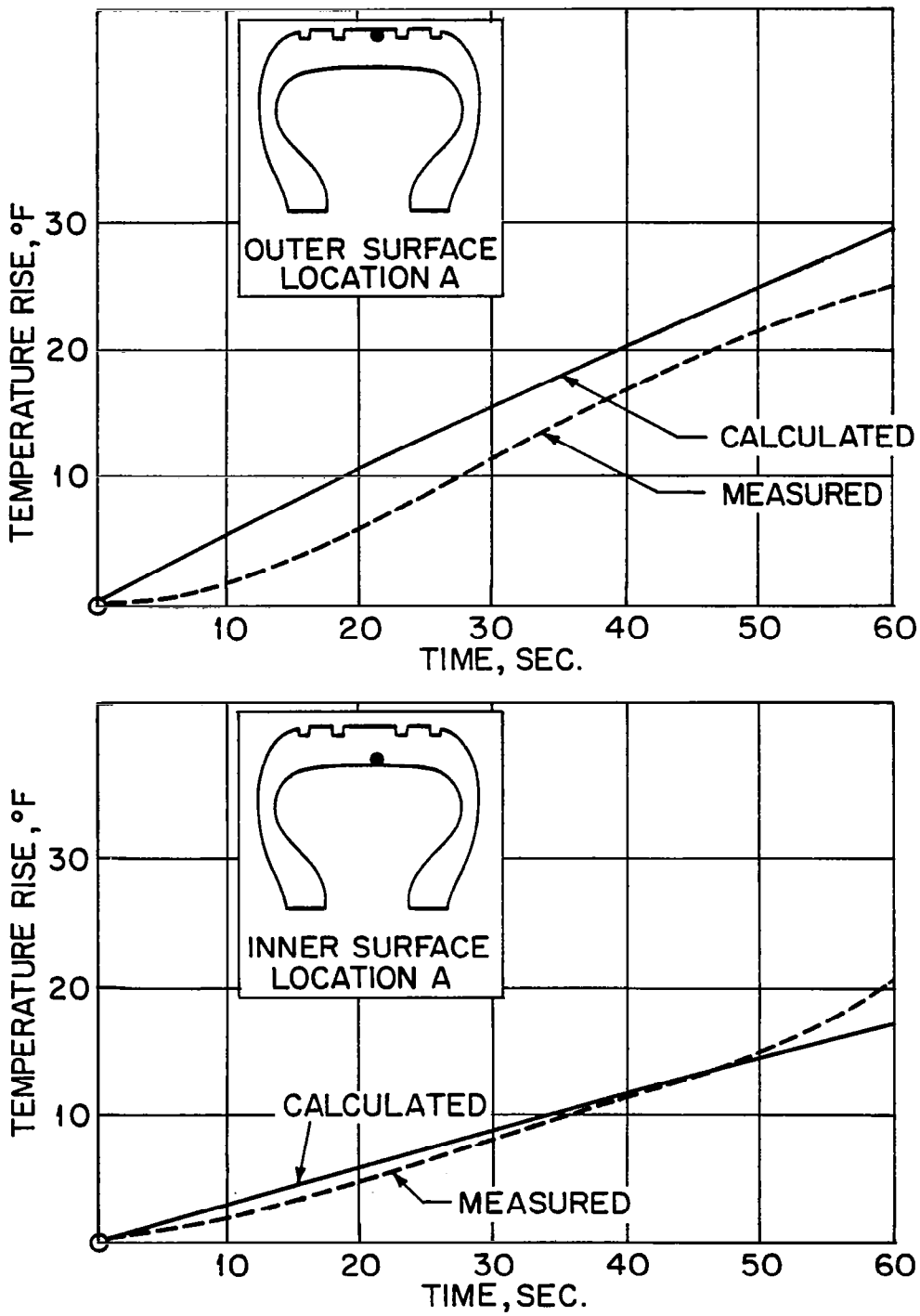

Fig. 29 Calculated and Measured Temperature Rise

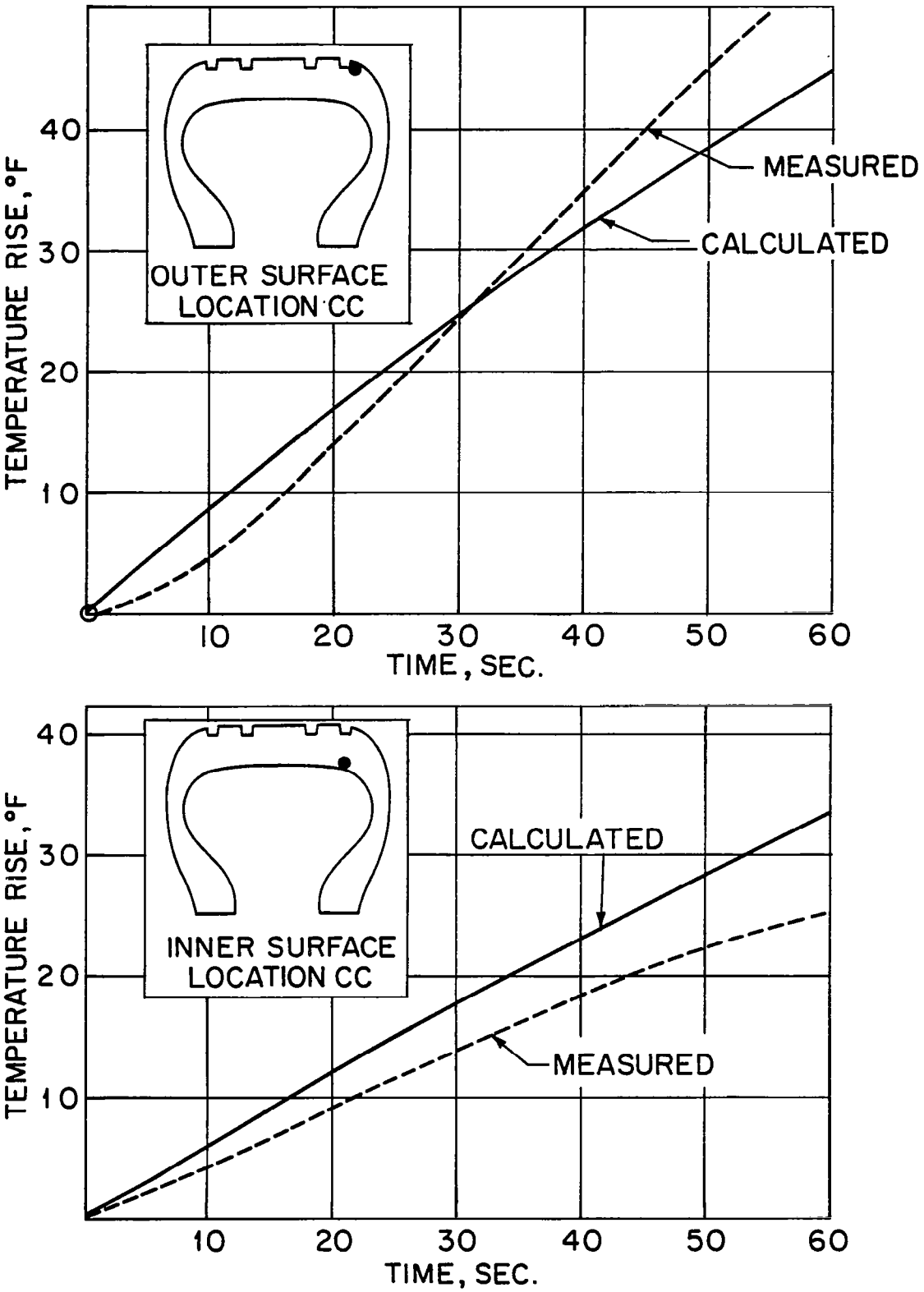

Fig. 30 Calculated and Measured Temperature Rise

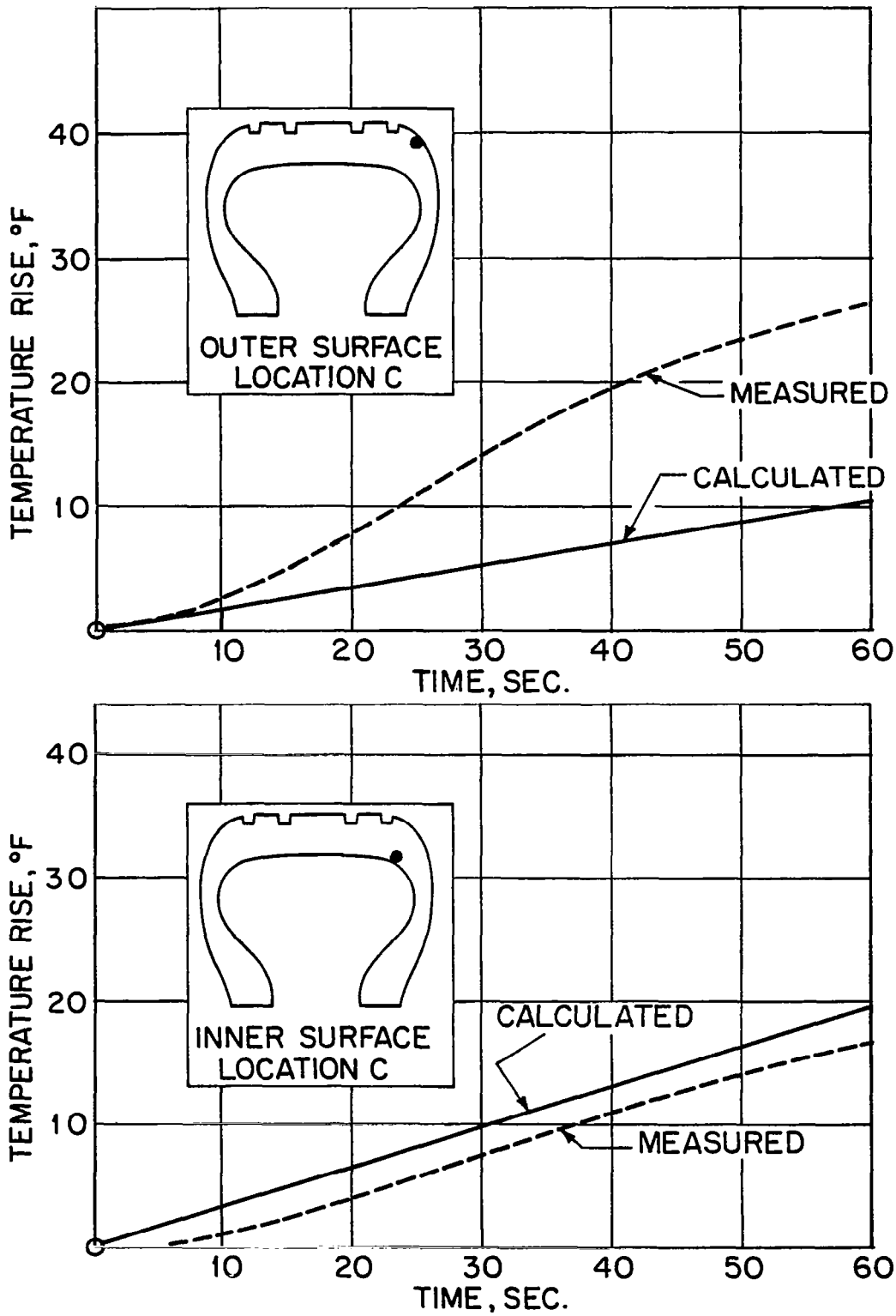

Fig. 31 Calculated and Measured Temperature Rise

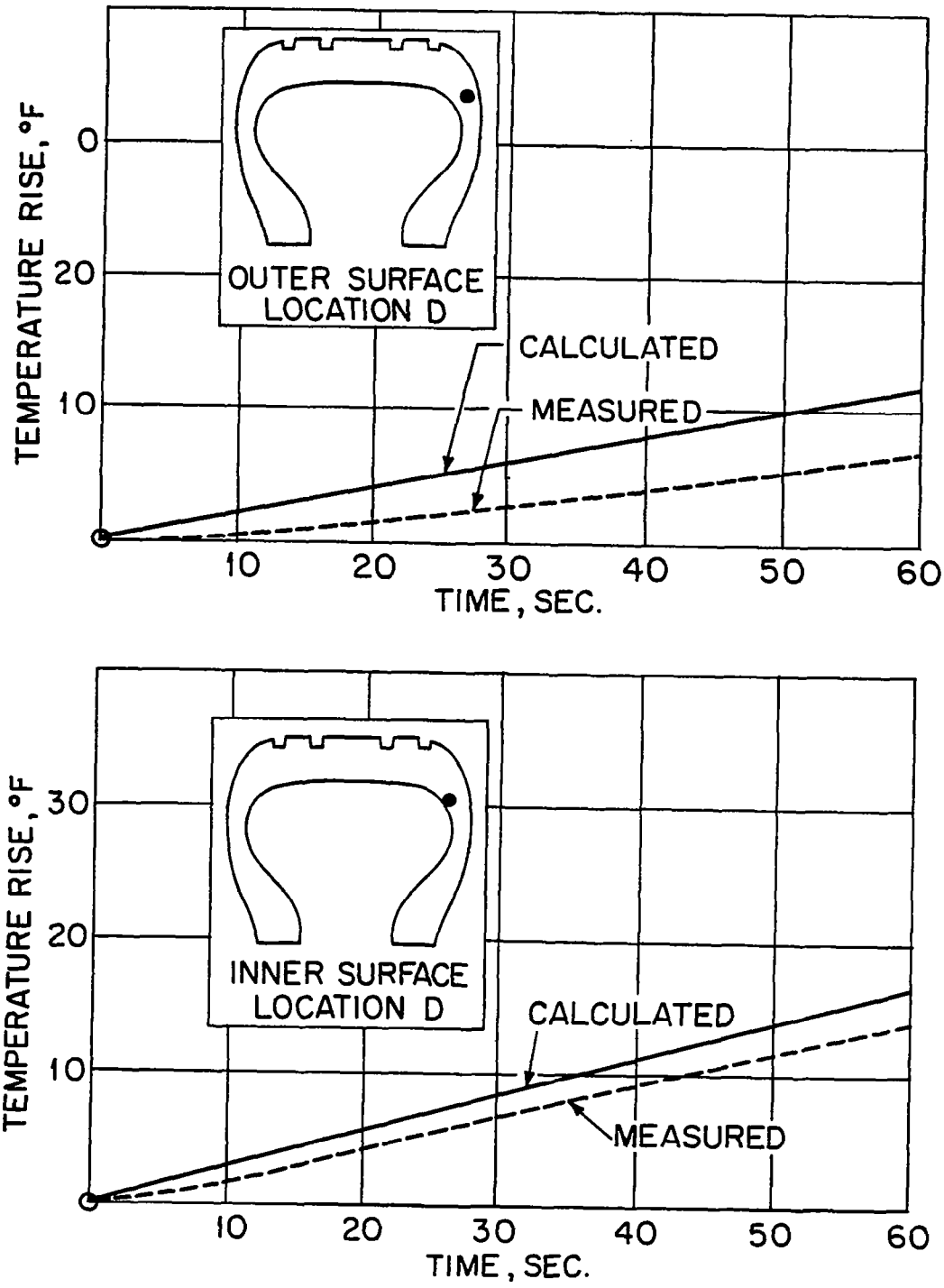

Fig. 32 Calculated and Measured Temperature Rise

for the fact that this region comes into contact with the runway surface because of the vertical sinkage during braking.

During one of the tests in the University of Michigan program a special sequence was added to the test procedure to investigate the cool-down effects of a 40 x 14, 28 PR tire after going through a braked rolling test. This was accomplished by continuing to record the temperature measurements after the brake test had been concluded and the tire retracted from the dynamometer surface. Also, after one minute of stationary cooling, a blower system was used to increase the cooling rate of the tire. Plots of several locations for a typical braked rolling-unload-cool down test run are shown in figure 33. As can be seen, there is generally a limited exponential type decay of temperature once the tire is unloaded. In some regions the decay is immediate while in others there is a short period of continued rise and then a decay. Again there is reasonably good correlation between the measured and calculated values even though the analytical model had not been specifically formulated for this situation.

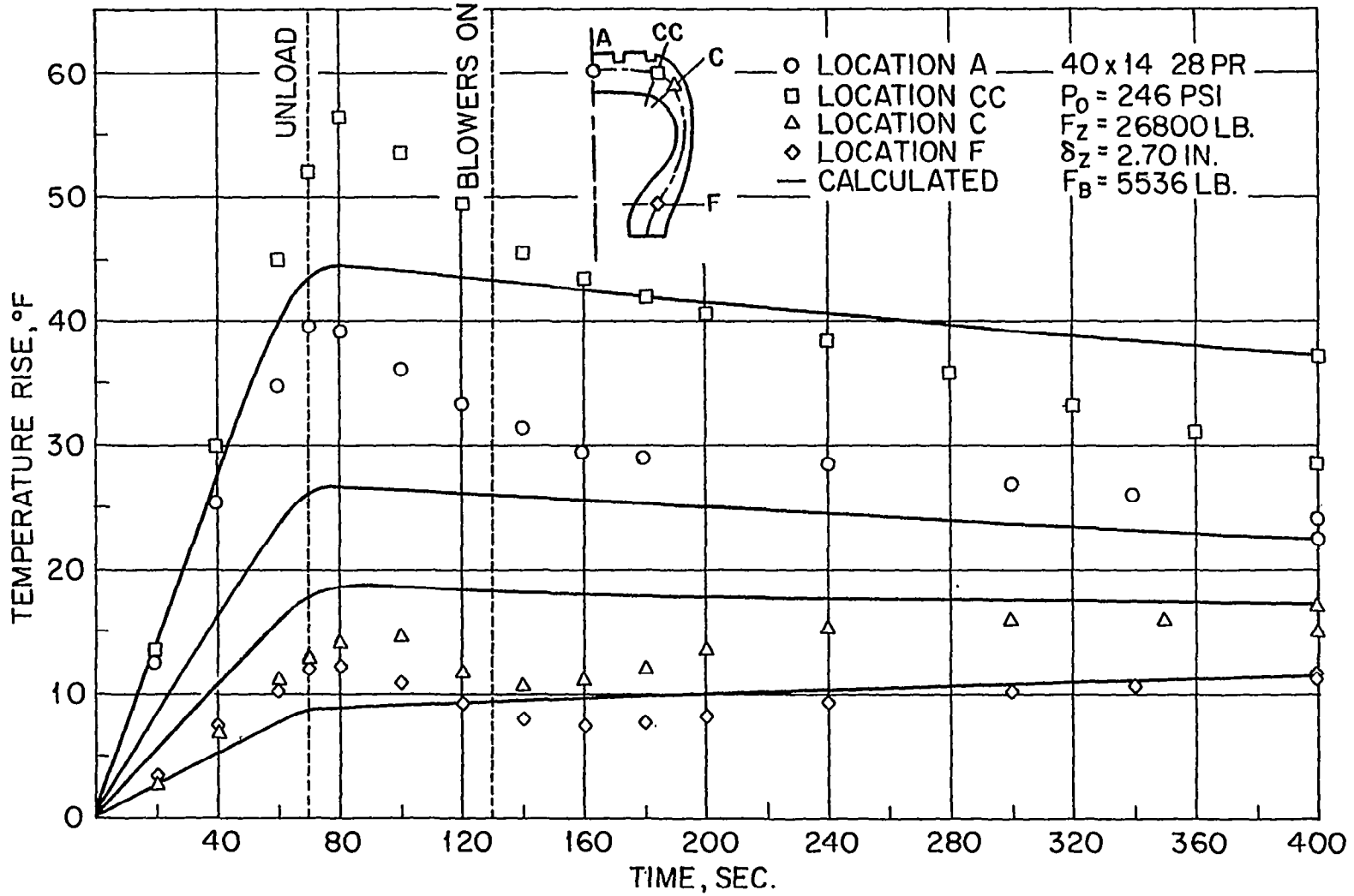

Fig. 33 Calculated and Measured Curves for Braked Rolling Followed by Static Cooling

REFERENCES

1. Clark, S. K., Dodge, R. N.: "Heat Generation in Aircraft Tires Under Free Rolling Conditions". NASA CR-3629, 1983.

2. Tanner, John A.: Fore-and-Aft Elastic Response Characteristics of 34 x 9.9, Type VII, 14 Ply-Rating Aircraft Tires of Bias-Ply, Bias-Belted, and Radial-Belted Design. NASA TN D-7449, 1974.

3. McCarty, John L.: "Wear and Related Characteristics of an Aircraft Tire During Braking". NASA TN D-6963, 1972.

CONCLUDING REMARKS

The influence of brake force on the heating of an aircraft tire is studied and equations for predicting this effect are derived in terms of the tire properties, such as size and spring rates, and the external brake force generated. Experments on tire heating due to braking show reasonable agreement with the predictions.

1. Report No.	2. Government Accession No.	3. Recipient's Catalog No.
NASA CR-3768		

4. Title and Subtitle	5. Report Date
HEAT GENERATION IN AIRCRAFT TIRES UNDER BRAKED ROLLING CONDITIONS	January 1984
	6. Performing Organization Code
7. Author(s)	8. Performing Organization Report No.
Samuel K. Clark and Richard N. Dodge	
	10. Work Unit No.
9. Performing Organization Name and Address	
Department of Mechanical Engineering and Applied Mechanics University of Michigan Ann Arbor, MI 48109	11. Contract or Grant No. NSG-1607
	13. Type of Report and Period Covered
12. Sponsoring Agency Name and Address	Contractor Report
National Aeronautics and Space Administration Washington, DC 20546	14. Sponsoring Agency Code

15. Supplementary Notes

Langley Technical Monitor: John Tanner

16. Abstract

An analytical model has been developed to approximate the internal temperature distribution in an aircraft tire operating under conditions of unyawed braked rolling. The model employs an array of elements to represent the tire cross-section and considers the heat generated within the tire to be caused by the change in strain energy associated with cyclic tire deflection. The additional heating due to tire slip and stresses induced by braking are superimposed on the previously developed free rolling model.

An extensive experimental program was conducted to verify temperatures predicted from the analytical model. Data from these tests were compared with calculations over a range of operating conditions. The model results were in reasonably good agreement with measured values.

17. Key Words (Suggested by Author(s))	18. Distribution Statement
Tire Heating Tire Braking	Unclassified - Unlimited Subject Category 39

19. Security Classif. (of this report)	20. Security Classif. (of this page)	21. No. of Pages	22. Price
Unclassified	Unclassified	56	A04

For sale by the National Technical Information Service, Springfield, Virginia 22161

NASA-Langley, 1984